

DFT study of hydrogen bonding between metal hydroxides and organic molecules containing N, O, S, and P heteroatoms: clusters vs. surfaces

Lea Gašparič^{a,b}, Matic Poberžnik^{a,1}, Anton Kokalj^{a,b,*}

^a Department of Physical and Organic Chemistry, Jožef Stefan Institute, Jamova 39, SI-1000 Ljubljana, Slovenia

^b Jožef Stefan International Postgraduate School, Jamova 39, SI-1000 Ljubljana, Slovenia

ARTICLE INFO

Keywords:

Hydrogen bond
Adsorption
Hydroxylated surfaces
Cluster and slab models
DFT calculations

ABSTRACT

Hydrogen bonds between either a water molecule or metal hydroxides and small organic molecules with functional groups that contain N, O, S, or P heteroatoms were analyzed using DFT calculations to shed some light on the question of whether hydroxylated nanoparticles and surfaces can be stabilized with organic molecules via hydrogen bonding interactions. Two different models of metal hydroxides were used, that is, small discrete clusters and periodic slab models of surfaces, where $\text{Al}(\text{OH})_3$ and $\text{Cu}(\text{OH})_2$ served as model systems. For small discrete cluster models, formula units of $\text{Al}(\text{OH})_3$ and $\text{Cu}(\text{OH})_2$ were taken, whereas for extended surface models, boehmite- $\text{AlOOH}(010)$ and $\text{Cu}(\text{OH})_2(001)$ surfaces were used. According to our results, the $\text{Cu}(\text{OH})_2$ cluster is usually a better H-bond acceptor and donor than the water molecule, whereas the $\text{Al}(\text{OH})_3$ cluster prefers to either act as an H-bond donor or to form two H-bonds, one as an H-bond donor and the other as an H-bond acceptor. Among the considered organic molecules with functional groups containing N, O, S, or P heteroatoms, imidazole and $(\text{CH}_3)_2\text{POOH}$ form the strongest H-bonds; the two molecules are very good H-bond acceptors as well as H-bond donors. These two molecules were also used to analyze hydrogen bonding with the boehmite- $\text{AlOOH}(010)$ and $\text{Cu}(\text{OH})_2(001)$ surfaces. The comparison between the surface and small-cluster calculations reveals that although cluster calculations can give reasonable estimates of adsorption energy provided that all formed H-bonds are properly accounted for (which is not always trivial), there are nevertheless structural intricacies—such as additional H-bonds with second-neighbor OH groups that may form on surfaces—that cannot be captured with small clusters. The more realistic aqueous conditions were also analyzed using the continuum solvation model. They not only influence the properties of H-bonds that are usually shorter than in vacuum but also induce deprotonation of adsorbed molecules, as observed for $(\text{CH}_3)_2\text{POOH}$ on a $\text{Cu}(\text{OH})_2$ surface.

1. Introduction

Since its first mention in a chemistry book by Lewis in 1923 [1], the H-bond has been the point of interest of many scientists. In early descriptions, the H-bond was considered to be a mostly ionic or electrostatic interaction [2] but later on, it was shown that it also exhibits a partially covalent character [3,4]. Gilli and co-workers have proposed an electrostatic-covalent H-bond model (ECHBM) [4], according to which the covalent nature of the H-bond varies with its strength; weak H-bonds are mostly electrostatic, whereas stronger H-bonds also have a covalent character. Weak H-bonds have a strength of up to about 0.2 eV,

moderate to strong H-bonds from about 0.2 to 0.65 eV, and very strong H-bonds up to 1.7 eV [5]. An H-bond can be designated as $\text{X}\cdots\text{H}\cdots\text{Y}$, where $\text{X}\cdots\text{H}$ is the donor group and Y is the acceptor. The strength of the H-bond depends on the type of the donor and acceptor groups and, in addition, also on the surrounding groups, hybridization [6–8], and acidity of the hydrogen atom [9]. Herein, we investigate moderate to strong conventional H-bonds, with X and Y atoms being O, N, and S. To a lesser extent, weak nonconventional $\text{CH}\cdots\text{O}$ bonds are also addressed.

H-bonds are not only a subject of academic interest in molecular chemistry, but are also relevant for applications in materials science (e.g., functionalization of surfaces and nanoparticles), catalysis, and

* Corresponding author at: Department of Physical and Organic Chemistry, Jožef Stefan Institute, Jamova 39, SI-1000 Ljubljana, Slovenia.

E-mail address: tone.kokalj@ijs.si (A. Kokalj).

URL: <http://www.ijs.si/ijsw/K3-en/Kokalj> (A. Kokalj).

¹ Present address: CNR-IOM Democritos National Simulation Center, c/o SISSA, via Bonomea 265, IT-34136 Trieste, Italy.

corrosion. For example, surfaces and nanoparticles can be stabilized and functionalized with suitable molecules. However, many surfaces are hydroxylated in the aqueous phase and gas phase under humid ambient conditions. In such cases, one of the possible molecular adsorption modes is via the formation of H-bonds between molecular adsorbates and surface OH groups [10–14]. The primary purpose of this paper is to explore such H-bonding interactions using molecular modeling based on density functional theory (DFT). To this end, we consider small organic molecules with functional groups containing N, O, S, and P heteroatoms because such functional groups are known as potent anchors for bonding to surfaces. For metal hydroxides, we consider discrete $\text{Al}(\text{OH})_3$ and $\text{Cu}(\text{OH})_2$ clusters as well as extended boehmite- $\text{AlOOH}(010)$ and $\text{Cu}(\text{OH})_2(001)$ surfaces. Yet in the aqueous environment, molecules that can form H-bonds can form them with either water molecules or OH groups present on materials surfaces. For this reason, we also investigate H-bonds between such molecules and a water molecule.

Concerning the effect of different metal ions on the strength of H-bonds, there are some general rules. In particular, the donor ability of metal hydroxides can be described with a synergetic effect [15–17], whereas their acceptor ability mainly depend on their gas-phase basicity [18,19]. The ability of aluminum oxides and hydroxides—such as Al_2O_3 , gibbsite $\text{Al}(\text{OH})_3$, and boehmite AlOOH —to form H-bonds with water molecules has already been extensively researched using DFT calculations, including ab initio molecular dynamics [20–24]. Boehmite surface, when exposed to water, shows extended H-bonding with water molecules due to a high degree of conformational freedom of surface OH groups [24]. Any defects present on the surface increase the strength of H-bonds [25]. Additionally, the adsorption of molecules—such as carboxylic, phosphonic, and amino acids as well as silanols—to these surfaces has also been investigated [13,14,26–30]. In an aqueous solvent, the molecules compete with water molecules for adsorption. These studies showed that such molecules could adsorb either in the so-called outer- or inner-sphere modes. The outer-sphere adsorption involves only molecule–surface H-bonds, whereas in the inner-sphere adsorption that is usually more stable, one or more strong molecule–surface O–Al chemical bonds are formed, and the molecule is additionally stabilized with H-bonds to the surface. In contrast to oxidized aluminum surfaces, H-bonding interactions with oxidized and hydroxylated copper surfaces have been much less investigated. Yu et al. [31,32] investigated the interaction of water molecules on CuO and Cu_2O surfaces and showed that the molecules can either adsorb through O–Cu bond and additional H-bonds, or dissociate and eventually form a hydroxylated surface. Similar adsorption modes were also reported for adsorption of methylphosphonic acid on hydroxylated Cu and Cu_2O surfaces [33].

To better appreciate the differences in H-bonding interactions between molecules and those between molecules and extended surfaces, we pursue herein an incremental systematic approach and first consider hydrogen bonding of small organic molecules with a water molecule, then illuminate the interaction of these molecules with small discrete metal hydroxide clusters, and finally pass to hydroxylated surfaces. In addition, H-bonds between molecules and metal hydroxides are also analyzed under more realistic aqueous conditions using a continuum solvation model. In the end, the relation between the H-bond energy and H-bond length is also evaluated. A better understanding of hydrogen bonding and adsorption on hydroxylated surfaces can give us some information about the potential of various molecules to either functionalize the surfaces or to act as corrosion inhibitors. Furthermore, the consideration of both discrete clusters and extended surfaces can also illuminate the question of whether the simplified calculations that utilize small discrete clusters can be used to approximately describe the H-bonding interactions between small organic molecules and hydroxylated metal surfaces.

2. Technical details

Calculations were performed in the framework of DFT using the

generalized gradient approximation (GGA) of Perdew–Burke–Ernzerhof (PBE) [34] with ultrasoft pseudopotentials [35,36] and a plane-wave basis set with the kinetic energy cutoff of 35 Ry (280 Ry for the charge density cutoff). The PWscf code from the QUANTUM ESPRESSO distribution [37,38] was used. The PBE method was chosen because for periodic plane-wave calculations, it represents the canonical GGA method. To account for weak dispersion interactions, a D3 semi-empirical dispersion correction of Grimme [39] with zero damping was also used; the results obtained by this scheme are denoted by the PBE-D3 label.

The results presented herein correspond to the PBE method unless explicitly indicated otherwise.

2.1. Molecular calculations

For plane-wave PBE calculations of molecular complexes and discrete clusters, we used the “*molecule in a box*” approach with a large cubic box of 24 Å in size, Gamma k-point, and the Makov–Payne [40] correction.

To evaluate the accuracy of PBE calculations, we also performed CCSD (coupled-cluster single-double) [41] calculations with an all-electron localized def2-TZVP basis set [42] using the Gaussian16 program [43]. Basis set superposition errors (BSSE) were estimated using a Boys–Bernardi counterpoise correction [44,45]. To make the comparison between the two methods more direct, PBE calculations were also made with the def2-TZVP basis set. While CCSD calculations were done only for complexes that involve water and/or ammonia molecules, PBE/def2-TZVP calculations were also performed for other considered molecular and cluster structures (these PBE/def2-TZVP results are presented in the Supplementary material).

By default, the PBE results presented herein correspond to the plane-wave basis set unless otherwise indicated, i.e., the label PBE corresponds to the PBE/plane-waves method and the label PBE-D3 corresponds to the PBE-D3/plane-waves method.

The discrete $\text{Cu}(\text{OH})_2$ cluster contains an odd number of electrons, hence spin-polarized calculations were performed for systems involving this cluster.

2.2. Adsorption calculations

For the adsorption calculations, the surfaces of boehmite- AlOOH and $\text{Cu}(\text{OH})_2$ were considered, in particular, $\text{AlOOH}(010)$ and $\text{Cu}(\text{OH})_2(001)$. AlOOH consists of HO–AlOOAl–OH multi-layers that extend in the (010) plane and are linked to one another via H-bonds, hence $\text{AlOOH}(010)$ is created by cutting only H-bonds in-between the adjacent double-layers. $\text{Cu}(\text{OH})_2$, on the contrary, consists of rows running along the (001) plane that are interlinked along and normal to the (001) plane with H-bonds, hence $\text{Cu}(\text{OH})_2(001)$ is also created by cutting only H-bonds. For the orthorhombic lattice parameters of the boehmite- AlOOH bulk, we used the calculated values of $a = 2.89$ Å, $b = 12.09$ Å, and $c = 3.73$ Å from our previous publication [29] and then cut the $\text{Al}(\text{OH})_3(010)$ slab, whereas the $\text{Cu}(\text{OH})_2(001)$ slab was built from the experimental structure of the $\text{Cu}(\text{OH})_2$ bulk [46] by cutting the (001) slab and then optimizing the two primitive unit-cell lattice vectors of $\text{Cu}(\text{OH})_2(001)$; the resulting primitive unit-cell lattice parameters are $a = b = 5.40$ Å.

To minimize lateral interactions between adsorbed molecules—the aim herein is to describe the H-bonds between the molecule and the surface—relatively large surface supercells were used. The sizes and shapes of the supercells as well as the thicknesses of the utilized slabs are shown in Fig. S1 in the Supplementary material. Brillouin zone integrations were performed with a shifted $1 \times 1 \times 1$ k-point grid for the supercell of $\text{AlOOH}(010)$ and with a shifted $2 \times 2 \times 1$ k-point grid for the supercell of $\text{Cu}(\text{OH})_2(001)$. For the latter, the Marzari–Vanderbilt cold smearing [47] of 0.01 Ry was also employed.

2.3. Aqueous phase calculations

A subset of calculations was also performed in the aqueous-phase with the solvent described implicitly using the `Environ` plugin [48] for `QUANTUM ESPRESSO` and the soft-sphere-continuum-solvation (SoftCS) implicit-solvent method [49].

2.4. Binding energy and charge density difference

The binding energy (E_b) between the two moieties forming a complex was used as a measure of the H-bond strength, i.e.:

$$E_b = E_{A-B} - (E_A + E_B), \quad (1)$$

where E_{A-B} is the total energy of the optimized A-B complex, and E_A and E_B are the total energies of the optimized standalone A and B moieties, respectively. For molecular complexes, A and B correspond to two molecules, whereas for adsorption calculations, A and B correspond to a surface and a molecule.

In cases where the most stable structure of an H-bonded complex consists of multiple H-bonds between A and B, individual H-bond strengths were calculated by considering less stable optimized A-B structures with only a single H-bond, where the structures of standalone A and B compatible with the inferior structure of A-B were also used. This concept is shown schematically in Fig. S2 in the Supplementary material.

H-bonds were also qualitatively characterized with the electron charge density difference, $\Delta\rho(\mathbf{r})$, calculated as:

$$\Delta\rho(\mathbf{r}) = \rho_{A-B}(\mathbf{r}) - \rho_A(\mathbf{r}) - \rho_B(\mathbf{r}), \quad (2)$$

where subscripts A, B, and A-B have the same meaning as above. Note, however, that in this case the structures of A and B were kept the same as in the A-B complex.

2.5. The denotation of H-bonded complexes

To distinguish which molecule in a complex is an H-bond donor and which an H-bond acceptor, H-bond complexes are designated as donor...acceptor. To help memorize the denotation, we use “XH→Y” as a mnemonic, where the arrow indicates that XH “donates” the H-bond to the Y acceptor. The denotation of H-bonds also follows the donor...acceptor nomenclature, i.e., H-bonds are always written as XH...Y and never as Y...HX.

In the case of the $(\text{CH}_3)_2\text{POOH}$ molecule, which has two groups capable of forming an H-bond, the group forming the H-bond is stated in the subscript, in particular: $(\text{CH}_3)_2\text{POOH}_{(\text{OH})}\cdots\text{acceptor}$ indicates that the OH group of $(\text{CH}_3)_2\text{POOH}$ is the H-bond donor, donor... $(\text{CH}_3)_2\text{POOH}_{(\text{OH})}$ indicates that the OH group is the H-bond acceptor, whereas donor... $(\text{CH}_3)_2\text{POOH}_{(\text{PO})}$ indicates that the P=O group is the H-bond acceptor.

2.6. Molecular graphics

Molecular graphics—i.e., molecular structures, adsorption structures, and electron charge density difference plots—were generated with `XCrySDen` [50], whereas assembling and postprocessing of figures was done with `Inkscape` [51].

3. Results and Discussion

In this section, we first compare the results of the PBE method with CCSD calculations to determine the accuracy of PBE results. Then we characterize hydrogen bonding between small organic molecules containing N, O, S, and P heteroatoms and a water molecule. In particular, we consider the following organic molecules:

- (i) N-containing molecules: CH_3NH_2 (sp^3 hybridized N atom), imidazole (aromatic molecule), and CH_2NH (sp^2 hybridized N atom);
- (ii) O-containing molecules: CH_3OH (sp^3 hybridized O atom) and CH_3CHO (sp^2 hybridized O atom);
- (iii) S-containing molecule: CH_3SH ;
- (iv) P-containing molecule: $(\text{CH}_3)_2\text{POOH}$.

The interaction of these molecules with the discrete $\text{Cu}(\text{OH})_2$ and Al $(\text{OH})_3$ clusters is characterized next and, finally, the adsorption of imidazole and $(\text{CH}_3)_2\text{POOH}$ on the boehmite- $\text{AlOOH}(010)$ and Cu $(\text{OH})_2(001)$ surfaces is presented.

3.1. $\text{H}_2\text{O} + \text{NH}_3$ benchmark: PBE vs. CCSD

As to establish the accuracy of the PBE method in describing hydrogen bonding, we compare its predictions with the benchmark results given by the CCSD method that is known to provide highly accurate results. To this end, we considered the $\text{H}_2\text{O}\cdots\text{H}_2\text{O}$, $\text{H}_2\text{O}\cdots\text{NH}_3$, and $\text{NH}_3\cdots\text{NH}_3$ complexes and the corresponding results are presented in Fig. 1. For the PBE calculations two different basis sets were used: plane-waves and def2-TZVP. The comparison between the PBE/def2-TZVP and CCSD/def2-TZVP results directly elucidates the accuracy of the PBE method and the comparison between PBE/plane-waves and PBE/def2-TZVP illuminates basis sets effects. While the plane-wave basis set usually gives slightly shorter hydrogen bonds than def2-TZVP,² the binding energies predicted by the two basis sets are very similar. In particular, the E_b values predicted by plane-waves usually fall within the ranges given by uncorrected and BSSE-corrected PBE/def2-TZVP values, as one would expect.

It can be seen from Fig. 1 that the PBE method gives the correct trend, although it predicts by about 0.05 eV too strong interactions, which is in agreement with the findings of Boese et al. [52]. These results suggest that the H-bond energies computed with PBE, though not highly accurate, can be used to ascertain H-bond acceptor and donor trends.

The geometry of H-bonded complexes is also shown in Fig. 1. The geometries of $\text{H}_2\text{O}\cdots\text{H}_2\text{O}$ and $\text{H}_2\text{O}\cdots\text{NH}_3$ complexes are similar for both methods, but the PBE distances are shorter than the CCSD distances, in accord with the slightly stronger H-bonds predicted by PBE. In contrast, considerable differences between PBE and CCSD appear for the structure of the $\text{NH}_3\cdots\text{NH}_3$ pair. While PBE predicts an H-bonded complex, CCSD does not. Interestingly, though, the intermolecular binding energies given by the two methods are nevertheless similar. While the CCSD calculated structure consists of two NH_3 molecules oriented in the opposite direction, in the PBE predicted complex, the N...H distance is 2.22 ± 0.01 Å and the NH...N angle is $166 \pm 1^\circ$, where \pm value indicates the differences between the two basis sets. It is known that NH_3 is a very good H-bond acceptor, but it has no propensity to act as an H-bond donor, [53] and this latter aspect is only predicted correctly by CCSD. We can therefore conclude that in the case of weak H-bonds the geometry computed with PBE may not be completely reliable.

3.2. H-bonds with a water molecule

We studied the interaction of a given organic molecule with a water molecule, where the organic molecule acted both as a donor and an acceptor of the H-bond. PBE/plane-waves optimized geometries of hydrogen-bonded complexes and the corresponding intermolecular binding energies are shown in Fig. 2, whereas the corresponding PBE/def2-TZVP results are presented in Fig. S3 in the Supplementary material. The H...Y bond lengths and the XH...Y angles are also stated, where

² For the water dimer and $\text{H}_2\text{O}\cdots\text{NH}_3$, the plane-wave basis set gives by 0.04 Å shorter hydrogen bonds than def2-TZVP, but for the ammonia dimer the two basis sets give very similar bond lengths.

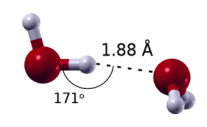
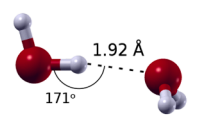
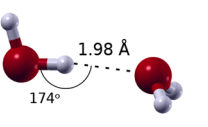

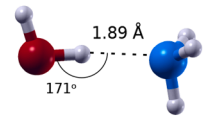
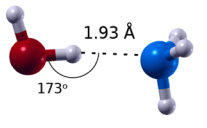
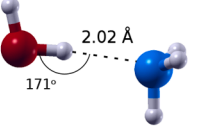
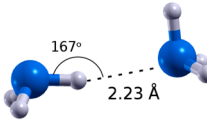
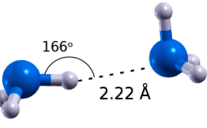
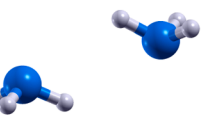
	PBE/plane-waves	PBE/def2-TZVP	CCSD/def2-TZVP	
H₂O...H₂O	 $E_b = -0.24$ eV	 $E_b = -0.27$ (-0.24) eV	 $E_b = -0.23$ (-0.20) eV	
H₂O...NH₃	 $E_b = -0.32$ eV	 $E_b = -0.34$ (-0.31) eV	 $E_b = -0.28$ (-0.24) eV	
NH₃...NH₃	 $E_b = -0.14$ eV	 $E_b = -0.17$ (-0.15) eV	 $E_b = -0.14$ (-0.11) eV	

Fig. 1. Optimized structures and intermolecular binding energies between water and ammonia molecules calculated with the PBE/plane-waves, PBE/def2-TZVP, and CCSD/def2-TZVP methods. Hydrogen bond lengths and angles are also stated. For the def2-TZVP basis set, the BSSE corrected binding energies are written in parentheses.

X and Y stand for the two heteroatoms involved in the hydrogen bond. In Fig. 2, the PBE-D3 binding energies are also reported (they are from 0.03 to 0.06 eV stronger than the PBE ones), whereas within the presented precision, the PBE-D3 geometries are identical to the PBE ones.

3.2.1. H-bonds with an N atom

N-containing molecules with different types of N atoms were considered: sp^3 hybridized (CH_3NH_2), aromatic (imidazole), and sp^2 hybridized (CH_2NH). If the water molecule acts as a donor, then the $H_2O \cdots CH_3NH_2$ bond is the strongest, while the bond with CH_2NH is the weakest (Fig. 2), thus following the $sp^3 > \text{aromatic} > sp^2$ trend of the bond strength, although the differences are small (within 0.05 eV). Instead, if the NH group acts as an H-bond donor, the H-bonds are weaker, and the H-bond with CH_3NH_2 does not even form. Imidazole forms a strong H-bond in both cases, and this can be attributed to conjugation and its aromatic character. These results are in good agreement with the previous studies of the effect of hybridization on the strength of the H-bond [6–8].

3.2.2. H-bonds with O and S atoms

O-containing molecules with two different types of O atoms were considered: sp^3 hybridized (CH_3OH) and sp^2 hybridized (CH_3CHO). In all considered cases, the H-bond strengths are very similar (Fig. 2), because the O atom acts both as a donor and an acceptor of the H-bond. It is worth noting that the $H_2O \cdots CH_3CHO$ complex also has a weak $CH \cdots O$ hydrogen bond that slightly enhances the binding energy, which is why E_b of $H_2O \cdots CH_3CHO$ is slightly more exothermic than that of $H_2O \cdots CH_3OH$, although it can be argued that the H-bond of the latter is somewhat stronger because it is slightly shorter (1.86 Å) than that of $H_2O \cdots CH_3CHO$ (1.87 Å) and also its H-bond angle (169°) is closer to the ideal 180° than that of $H_2O \cdots CH_3CHO$ (162°). Taking this into account, we may conclude that the sp^3 hybridized O atom should form slightly stronger H-bonds than the sp^2 hybridized O atom. This trend is thus similar to the one reported above for the N atom.

One molecule with the sp^3 hybridized S atom was also considered, CH_3SH (Fig. 2). Results reveal that a sulfur atom is a much better acceptor than a donor, which agrees with the findings of Raub and co-workers [54].

The results presented in Fig. 2 reveal the following trend of H-bond strengths between water and N-, O-, and S-containing molecules: $OH \cdots N > OH \cdots O > OH \cdots S$.

3.2.3. H-bonds with P=O and P–OH groups

As shown in Fig. 2, three different H-bonds between $(CH_3)_2POOH$ and H_2O are possible due to one donor OH group and two different acceptor O atoms in the $(CH_3)_2POOH$ molecule; one is a part of the hydroxyl group (OH), and the other is bonded to the phosphorus atom with the double bond (P=O). The H-bond with the P=O acceptor is considerably stronger ($E_b = -0.36$ eV) than the one with the OH acceptor ($E_b = -0.21$ eV), which is expected because the P=O group is known to be a very strong H-bond acceptor [55]. The OH group can also act as an H-bond donor and the corresponding hydrogen bond with the water molecule is very strong ($E_b = -0.36$ eV). In this complex, designated as $(CH_3)_2POOH_{(OH)} \cdots H_2O$, the $(CH_3)_2POOH$ molecule was constrained to a less stable geometry with the hydrogen atom of the OH group rotated around the P–O bond by 180° to ensure only a single H-bond between the molecule and H_2O forms; otherwise, two H-bonds would form, one with the OH group as a donor and the other with the P=O group as an acceptor (shown on the far right in Fig. 2).³ The H-bond energy of $(CH_3)_2POOH_{(OH)} \cdots H_2O$, reported in Fig. 2, was therefore calculated with respect to the energy corresponding to the less stable rotated OH group both in the complex and the standalone $(CH_3)_2POOH$ molecule.

Among the three possible H-bonds that can form between $(CH_3)_2POOH$ and H_2O , the $HOH \cdots O(H)P$ hydrogen bond is therefore considerably weaker than the $POH \cdots OH_2$ and $HOH \cdots O=P$ hydrogen bonds, which display similar stabilities. This trend is also clearly evident from the charge density difference plots, shown in Fig. 3. This figure shows that the charge redistributions in the $(CH_3)_2POOH_{(OH)} \cdots H_2O$ and $H_2O \cdots (CH_3)_2POOH_{(PO)}$ complexes have a similar pattern and intensity, whereas the charge redistribution in the $H_2O \cdots (CH_3)_2POOH_{(OH)}$ complex is weaker.

³ The corresponding binding energy for the $(CH_3)_2POOH/H_2O$ complex with two H-bonds is -0.62 eV.

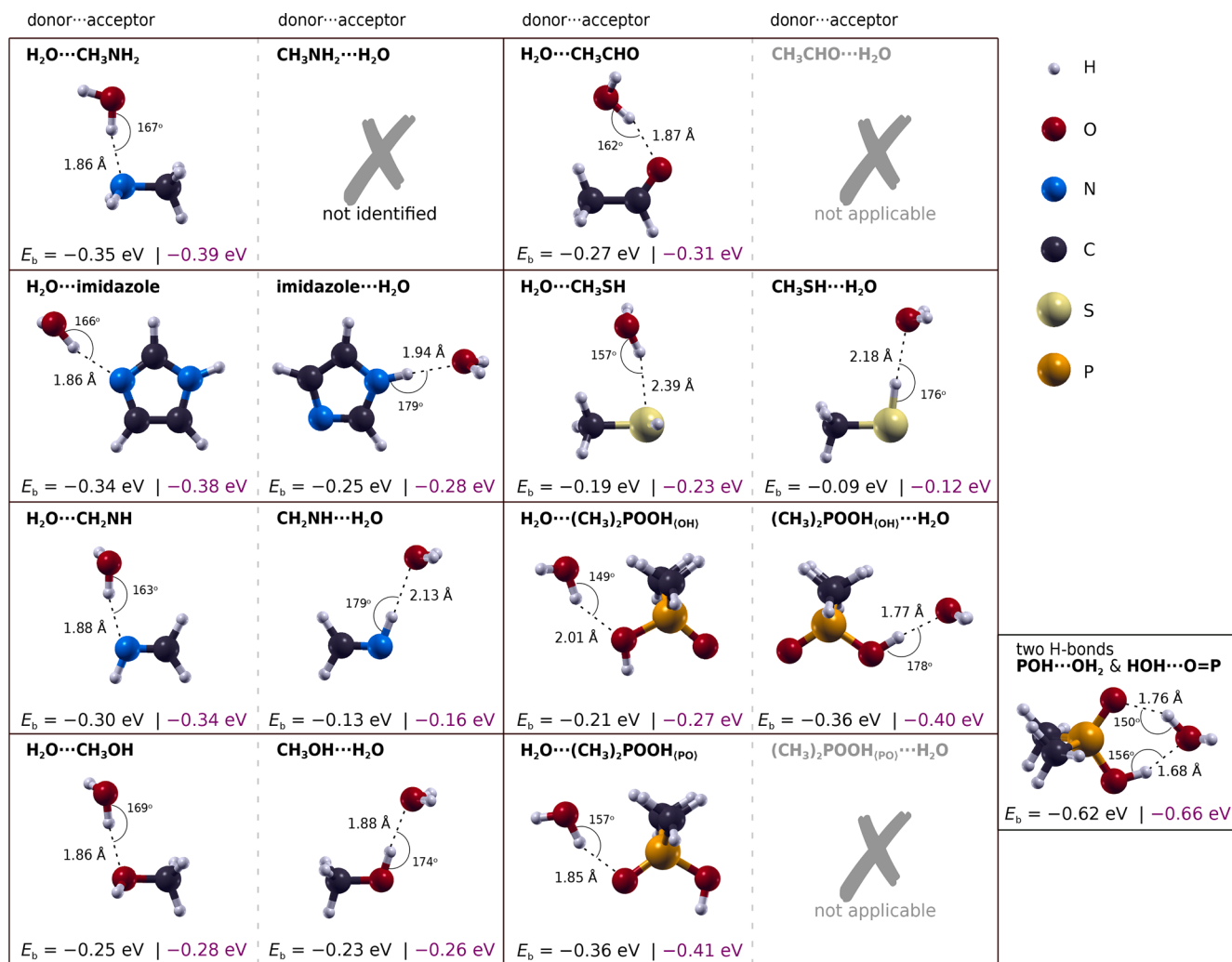


Fig. 2. The PBE optimized geometries, H-bond lengths and H-bond angles of the complexes between the considered organic molecules and a water molecule. In addition to the PBE binding energies, the PBE-D3 values are also reported as “PBE | PBE-D3”, with the PBE-D3 values written in purple. For each organic molecule, at least two configurations are considered: in the left structure, the organic molecule acts as the H-bond acceptor and in the right structure as the H-bond donor. Additionally, for (CH₃)₂POOH, the structure with two H-bonds is shown on the far right.

3.2.4. Molecular H-bond acceptor and donor propensities

The comparison of H-bond acceptor propensities among the investigated molecules shows that molecules with either an N atom or the P=O group are good acceptors, followed by molecules with an O atom bonded to C, whereas an S heteroatom displays the weakest acceptor propensity among the molecules considered in Fig. 2. The effect of hybridization is also apparent: an sp³ hybridized heteroatom has better acceptor abilities than an sp² hybridized atom of the same kind, whereas for donor propensities, the connection between the type of heteroatom and the H-bond strength is less straightforward.

Schwöbel and co-workers made a list of H-bond acceptor's strengths [59,60]. If we consider molecules investigated herein, the P=O group and amine are the best acceptors, followed by imidazole, imine, alcohol, aldehyde, and thiol. The same sequence is also predicted with the pK_a slide rule of Gilli et al. [9]. Our results are in excellent agreement with the anticipated order of acceptor strength. The donor propensity of the molecules also conforms to chemical expectations; it is the highest for an acidic OH group that is present in the (CH₃)₂POOH molecule, followed by alcohol, imidazole, and, finally, thiol [56].

H-bonds with the (CH₃)₂POOH molecule are stronger than the bonds with alcohol or aldehyde, the exception being the H₂O... (CH₃)₂POOH(OH) hydrogen bond, which is weaker than the analogous one between methanol and H₂O. The phosphorous atom appears to have

an opposing effect on the oxygen's acceptor propensity; the O atom in the P=O group is a much better acceptor than the normal ketone but the O atom of the P–OH group is a worse acceptor than the normal alcohol. As for the donor propensity, the OH group of (CH₃)₂POOH is a much better donor than the OH group of methanol.

Current results are compared with data from the literature in Table 1. The energies from different sources show some deviations due to different computational details. Our calculated H-bonds are slightly stronger than those from the literature that were calculated with the MP2 method, but the trend is rather well reproduced. This is expected if we take into account the comparison between the results given by the PBE and CCSD methods (Fig. 1).

As for the comparison between PBE/plane-waves and PBE/def2-TZVP results, it can be observed from Table 1 that the *E_b* values predicted by plane-waves usually fall within the ranges, given by uncorrected and BSSE-corrected PBE/def2-TZVP values, as one would expect.

3.3. H-bonds with a discrete Cu(OH)₂ cluster

Next, we consider hydrogen bonding between a discrete Cu(OH)₂ cluster and organic molecules; here, the set of molecules is the same as the one considered above for a water molecule. PBE/plane-waves optimized structures of the resulting hydrogen-bonded complexes are shown

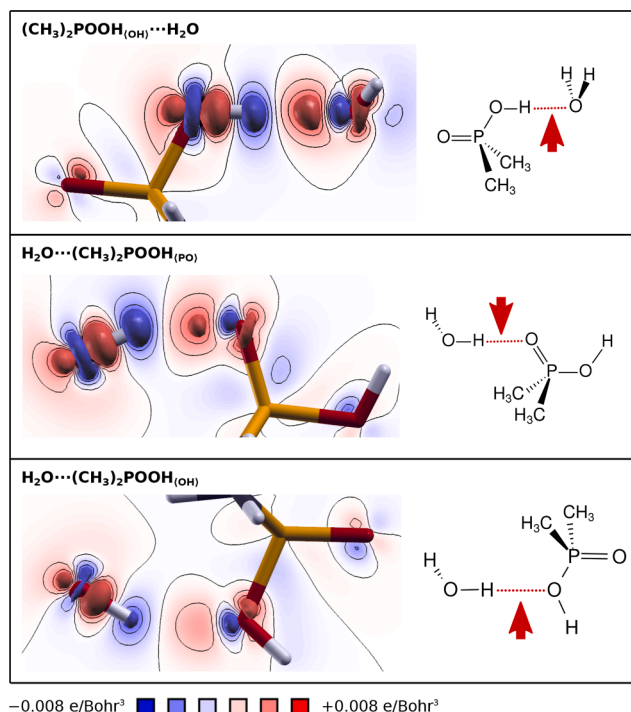


Fig. 3. The electron charge density difference, $\Delta\rho(r)$, for the three possible H-bonds that can form between the $(\text{CH}_3)_2\text{POOH}$ and H_2O molecules. For each case, the H-bond visualized in the $\Delta\rho(r)$ plot (left) is indicated by the red arrow on the schematic skeleton structure (right). Isosurfaces of $\pm 0.005 \text{ e/Bohr}^3$ are shown, whereas contours are drawn in a linear scale from -0.008 to $+0.008 \text{ e/Bohr}^3$ with an increment of 0.002 e/Bohr^3 .

Table 1

The comparison of the currently calculated binding energies to those reported in the literature for H-bonded complexes with a water molecule. The BSSE corrected binding energies are written in parentheses.

donor ... acceptor	E_b (eV)		
	PBE/plane-waves	PBE/def2-TZVP	literature
$\text{H}_2\text{O} \cdots \text{CH}_3\text{NH}_2$	-0.35	-0.36 (-0.32)	-0.29 ^a , (-0.33) ^b
$\text{H}_2\text{O} \cdots \text{imidazole}$	-0.34	-0.35 (-0.31)	-0.30 ^a , (-0.34) ^b
$\text{imidazole} \cdots \text{H}_2\text{O}$	-0.25	-0.29 (-0.27)	-0.23 ^a , (-0.27) ^b
$\text{H}_2\text{O} \cdots \text{CH}_2\text{NH}$	-0.30	-0.31 (-0.27)	-0.29 ^c
$\text{CH}_2\text{NH} \cdots \text{H}_2\text{O}$	-0.13	-0.17 (-0.14)	-0.14 ^c , (-0.13) ^b
$\text{H}_2\text{O} \cdots \text{CH}_3\text{OH}$	-0.25	-0.27 (-0.23)	-0.22 ^a , (-0.21) ^d
$\text{CH}_3\text{OH} \cdots \text{H}_2\text{O}$	-0.23	-0.27 (-0.23)	-0.20 ^a , (-0.19) ^d
$\text{H}_2\text{O} \cdots \text{CH}_3\text{CHO}$	-0.27	-0.28 (-0.25)	-0.22 ^a
$\text{H}_2\text{O} \cdots \text{CH}_3\text{SH}$	-0.19	-0.22 (-0.19)	-0.16 ^a
$\text{CH}_3\text{SH} \cdots \text{H}_2\text{O}$	-0.09	-0.13 (-0.11)	-0.08 ^a , (-0.10) ^b

^a Rablen et al. [56] (B3LYP/6-31++G(2d(X+),p)//B3LYP/6-31+G(d(X+),p))

^b Raub et al. [54] (MP2/aug-cc-pVTZ).

^c Arey et al. [57] (MP2/aug-cc-pVTZ + W1 method).

^d Mandal et al. [58] (MP2/6-311++G(d,p))

in Fig. 4, along with the binding energies, H-bond lengths, and H-bond angles, whereas the corresponding PBE/def2-TZVP results are presented in Fig. S4 in the Supplementary material. In Fig. 4, the PBE-D3 binding energies are also reported (they are from 0.04 to 0.08 eV stronger than the PBE ones), whereas within the presented precision, the PBE-D3 geometries are identical to PBE ones, except for $\text{CH}_3\text{NH}_2 \cdots \text{Cu}(\text{OH})_2$ PBE-D3 gives by 0.01 Å shorter H-bond and by 1° larger H-bond angle.

Molecules containing either an N atom, an O atom bonded to C, or an S atom show stronger and shorter H-bonds with a $\text{Cu}(\text{OH})_2$ cluster than with a H_2O molecule. Even the $\text{CH}_3\text{NH}_2 \cdots \text{Cu}(\text{OH})_2$ complex is stable,

although the CH_3NH_2 molecule is a very poor H-bond donor, as discussed above. The only exception is the CH_3CHO molecule for which the binding energy with H_2O is marginally more exothermic than with $\text{Cu}(\text{OH})_2$. However, in this case, the reason for the more exothermic binding energy is not the stronger $\text{OH} \cdots \text{O}$ bond, but the additional stabilization provided by the weak $\text{CH} \cdots \text{O}$ bond in the $\text{H}_2\text{O} \cdots \text{CH}_3\text{CHO}$ complex (*vide supra*). This reasoning is supported by the $\text{OH} \cdots \text{O}$ bond length, which is shorter in $\text{Cu}(\text{OH})_2 \cdots \text{CH}_3\text{CHO}$ (1.83 Å) than in $\text{H}_2\text{O} \cdots \text{CH}_3\text{CHO}$ (1.87 Å). We can therefore deduce that the $\text{Cu}(\text{OH})_2$ cluster is a better H-bond acceptor and donor than the water molecule, but otherwise, the trend of the H-bond strength of various complexes with the $\text{Cu}(\text{OH})_2$ cluster is similar to that with the water molecule, except for CH_3NH_2 , which does not donate an H-bond to H_2O .

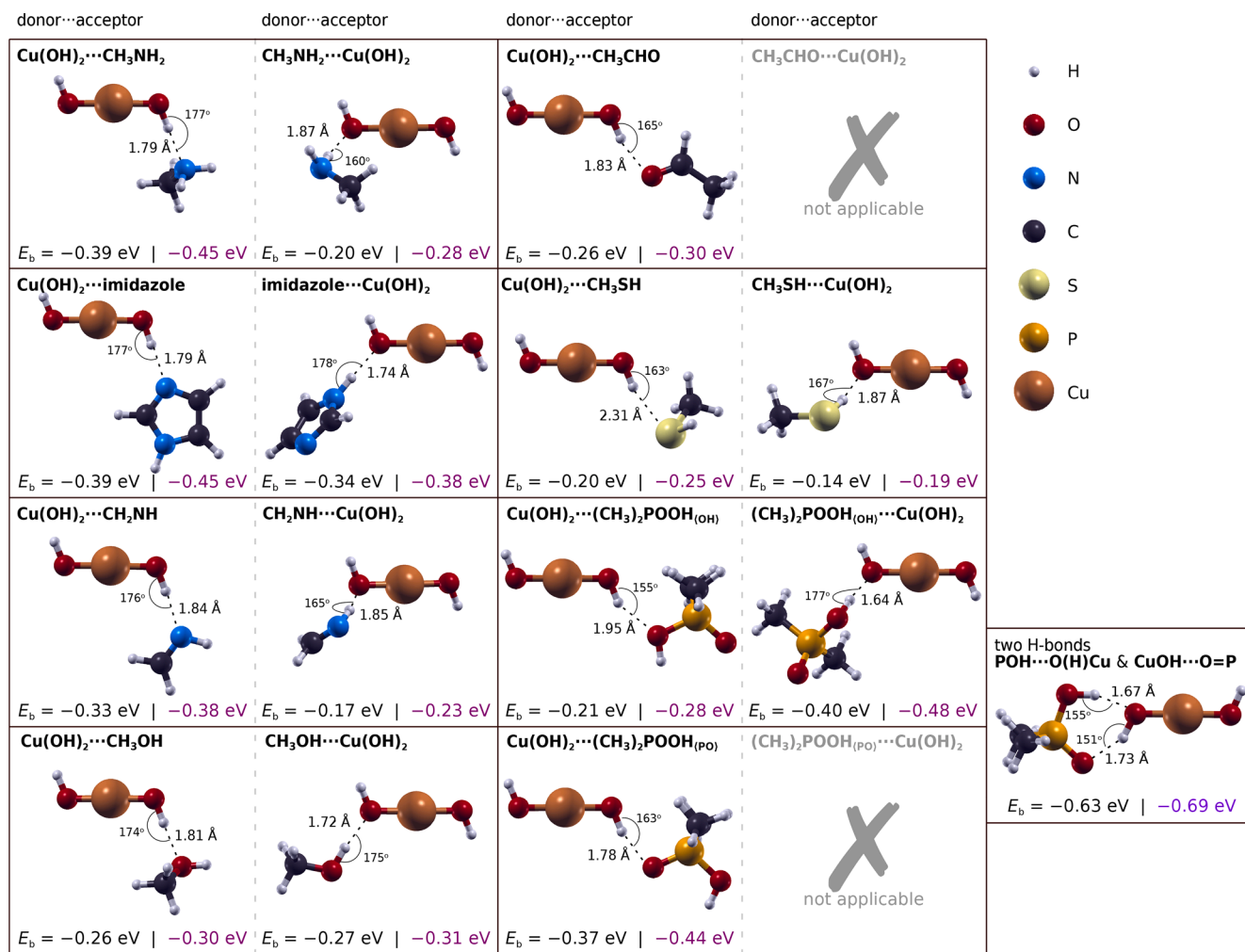
As for the complexes with $(\text{CH}_3)_2\text{POOH}$, three different H-bonds are possible (*vide supra*). For two of them (donor $\cdots (\text{CH}_3)_2\text{POOH}_{(\text{OH})}$ and donor $\cdots (\text{CH}_3)_2\text{POOH}_{(\text{PO})}$) the bond strengths given by the $\text{Cu}(\text{OH})_2$ and H_2O donors are very similar (within 0.01 eV). For the third type of hydrogen bond, $(\text{CH}_3)_2\text{POOH}_{(\text{OH})} \cdots$ acceptor, the H-bond strength with the $\text{Cu}(\text{OH})_2$ cluster is stronger than that with H_2O , the respective E_b values being -0.40 eV and -0.36 eV (note that the H-bond strength of $(\text{CH}_3)_2\text{POOH}_{(\text{OH})} \cdots \text{Cu}(\text{OH})_2$ was estimated with respect to the less stable rotated OH group of $(\text{CH}_3)_2\text{POOH}$, similarly as was done for $(\text{CH}_3)_2\text{POOH}_{(\text{OH})} \cdots \text{H}_2\text{O}$ above). According to binding energies, the bond strength trend for the three H-bonds is $\text{POH} \cdots \text{O}(\text{H})\text{Cu} > \text{CuOH} \cdots \text{O}=\text{P} > \text{CuOH} \cdots \text{O}(\text{H})\text{P}$. This trend is consistent with the H-bond lengths (in the sense that the stronger the bond, the shorter is the bond length) and the charge density differences (Fig. 5), which show that the magnitude of charge redistribution follows the same order.

In metal hydroxides, the OH group is bonded to the metal center. The free hydroxide ion is known to be a bad H-bond donor and an excellent acceptor [18], but a bond with a metal cation can affect these properties. In the case of the $\text{Cu}(\text{OH})_2$ cluster, the OH group's donor and acceptor propensities are better than the ones of the water molecule. This means that the donor propensity of the hydroxyl group in $\text{Cu}(\text{OH})_2$ is better, and the acceptor propensity is worse than that of the standalone hydroxide ion. The increase of the donor propensity can be explained with the synergetic effect [15–17] that attributes the increase of the donor propensity of the hydroxyl group to the M–O bonding interaction which weakens the O–H bond in the hydroxyl group. Small metal cations with a high charge and those that form covalent bonds show a strong synergetic effect. A similar concept can be applied to the acceptor propensity. The stronger M–O bond reduces the basicity of the OH group and therefore weakens its acceptor propensity.

3.4. H-bonds with a discrete $\text{Al}(\text{OH})_3$ cluster

In addition to the discrete $\text{Cu}(\text{OH})_2$ cluster, we also considered a discrete $\text{Al}(\text{OH})_3$ cluster and its propensity to form H-bonds. PBE/plane-waves results are shown in Fig. 6, whereas the corresponding PBE/def2-TZVP results are presented in Fig. S5 in the Supplementary material. In Fig. 6, the PBE-D3 binding energies are also reported (they are from 0.04 to 0.09 eV stronger than the PBE ones), whereas within the presented precision, the PBE-D3 geometries are identical to the PBE ones.

The binding energies of complexes where the $\text{Al}(\text{OH})_3$ cluster acts as a donor are similar to that of the $\text{Cu}(\text{OH})_2$ cluster. The majority of H-bonded $\text{Al}(\text{OH})_3$ complexes also contain weak $\text{CH} \cdots \text{O}$ hydrogen bonds which enhance the stability of the complex, hence caution should be exercised when drawing conclusions solely based on the binding energies. The energy of the $\text{CH} \cdots \text{O}$ bond depends not only on the bond distance and angle but also on the type of donor group [6,61], hence it is not straightforward to determine the contribution of the $\text{CH} \cdots \text{O}$ interaction to the overall binding energy. For this reason, we analyzed the dependence of the $\text{CH} \cdots \text{O}$ hydrogen bond on its length and angle (see Figs. S6 and S7 in the Supplementary material). H-bond energies ranging from -0.04 to -0.10 eV were obtained. When this contribution is taken

Fig. 4. Similar to Fig. 2, but for the H-bonded complexes with a discrete $\text{Cu}(\text{OH})_2$ cluster.

into account, we can argue that donor propensities of $\text{Cu}(\text{OH})_2$ and $\text{Al}(\text{OH})_3$ clusters are similar; in some cases, $\text{Cu}(\text{OH})_2$ may even be a slightly better donor.

Concerning the acceptor propensity of the $\text{Al}(\text{OH})_3$ cluster, the calculations revealed that a single H-bond with $\text{Al}(\text{OH})_3$ acting as the acceptor forms only for CH_3NH_2 and imidazole, whereas for other molecules the corresponding initial structures converged to a local minimum with two H-bonds where $\text{Al}(\text{OH})_3$ acted both as a donor and an acceptor. This indicates that $\text{Al}(\text{OH})_3$ is a better H-bond donor than acceptor. We can thus deduce that the low tendency of $\text{Al}(\text{OH})_3$ to act exclusively as H-bond acceptor is a consequence of its weaker acceptor propensity and its propeller-like structure, which allows for the formation of complexes with multiple H-bonds.

The complexes with two H-bonds, where $\text{Al}(\text{OH})_3$ acts as a donor and an acceptor, are also shown in Fig. 6. Their binding energies are similar to those where $\text{Al}(\text{OH})_3$ is a donor, except for $(\text{CH}_3)_2\text{POOH}$ (see below). For the CH_3NH_2 molecule, local minima were identified for all three types of complexes with $\text{Al}(\text{OH})_3$ acting either as a donor only, as a donor + acceptor, or as an acceptor only. This example shows that the binding energy of the complex with two H-bonds is not given by the sum of the two isolated H-bond energies, which precludes quantitative estimation of the acceptor propensity of $\text{Al}(\text{OH})_3$ from the difference between the binding energies of the complex with two H-bonds and that with $\text{Al}(\text{OH})_3$ acting as a donor only.

The tendency of the $\text{Al}(\text{OH})_3$ cluster to form two hydrogen bonds is the most pronounced with $(\text{CH}_3)_2\text{POOH}$ because their complexes with two H-bonds are considerably more stable than those with a single H-

bond; two such complexes between $\text{Al}(\text{OH})_3$ and $(\text{CH}_3)_2\text{POOH}$ with two H-bonds are shown in Fig. 6.

Each of the three possible H-bonds between $\text{Al}(\text{OH})_3$ and $(\text{CH}_3)_2\text{POOH}$ is analyzed using electron charge density difference in Fig. 7; these bonds are $\text{POH} \cdots \text{O}(\text{H})\text{Al}$, $\text{AlOH} \cdots \text{O}=\text{P}$, and $\text{AlOH} \cdots \text{O}(\text{H})\text{P}$. The first two of these H-bonds are analyzed for the same complex, which displays the binding energy of -0.73 eV in Fig. 6. While the pattern of electron charge redistribution is very similar for the first two H-bonds, the magnitude of redistribution is nevertheless slightly smaller for the $\text{AlOH} \cdots \text{O}=\text{P}$ hydrogen bond, in accord with its longer bond length of 1.71 \AA (for comparison the bond length of the other hydrogen bond, $\text{POH} \cdots \text{O}(\text{H})\text{Al}$, is 1.63 \AA). The magnitude of the electron charge redistribution is by far the smallest for the third H-bond, $\text{AlOH} \cdots \text{O}(\text{H})\text{P}$, in accord with its longer length of 1.93 \AA and weaker binding energy (-0.21 eV).

3.5. Molecular adsorption on the $\text{AlOOH}(010)$ and $\text{Cu}(\text{OH})_2(001)$ surfaces

To compare the results of the discrete cluster calculations with those obtained on more realistic systems, molecular adsorption via the formation of H-bonds between molecular adsorbates and surface OH groups was considered on the boehmite- $\text{AlOOH}(010)$ and $\text{Cu}(\text{OH})_2(001)$ surfaces. To this end, only imidazole and $(\text{CH}_3)_2\text{POOH}$ were used as adsorbates because these two molecules form strong H-bonds (*vide supra*) and, moreover, they are technologically relevant as either corrosion inhibitors or chelating agents.

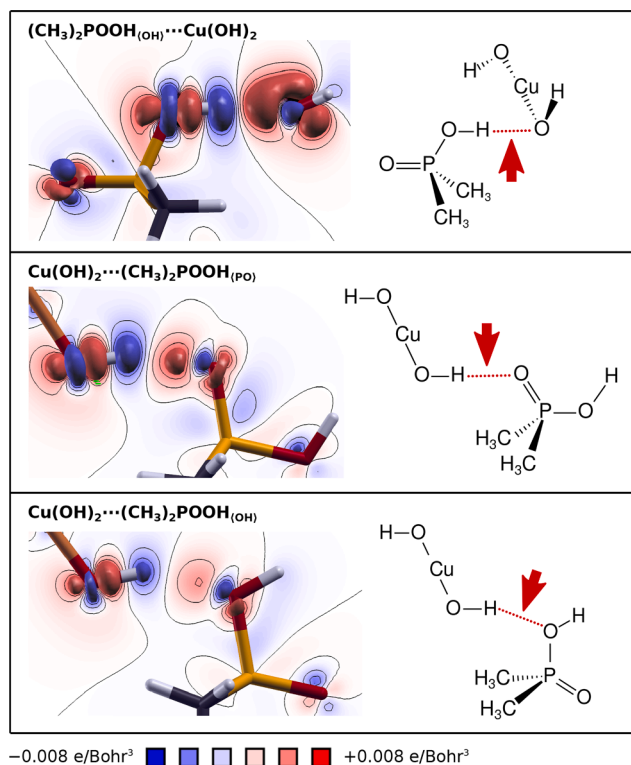


Fig. 5. The electron charge density difference, $\Delta\rho(r)$, for the three possible H-bonds that can form between $(\text{CH}_3)_2\text{POOH}$ and a discrete $\text{Cu}(\text{OH})_2$ cluster. For each case, the H-bond visualized in the $\Delta\rho(r)$ plot (left) is indicated by the red arrow on the schematic skeleton structure (right). Isosurfaces and contours are compatible with those shown in Fig. 3 (isosurfaces: ± 0.005 e/Bohr³; contours: from -0.008 to 0.008 e/Bohr³ with a linear increment of 0.002 e/Bohr³).

It should be noted that molecular adsorption on $\text{Cu}(\text{OH})_2(001)$ resulted in large distortions and symmetry lowering of the $\text{Cu}(\text{OH})_2(001)$ substrate. The corresponding binding energies were therefore calculated with respect to the total energy of the bare $\text{Cu}(\text{OH})_2(001)$ slab that was reoptimized after removing the adsorbed molecule. This assures that compatible structures of the molecule/slab and slab systems were used in the calculation of binding energies.

Identified adsorption structures and their binding energies are shown in Fig. 8. In addition to PBE binding energies, PBE-D3 values are also stated. While on cluster models, PBE-D3 binding energies are only slightly stronger than PBE ones (by less than 0.1 eV), PBE-D3 gives by about 0.3 eV stronger binding energies on surfaces. This PBE vs. PBE-D3 difference of 0.3 eV in adsorption binding energy is typical for molecules of the size of imidazole [62–64]. The reason that the PBE vs. PBE-D3 difference is much smaller on cluster than on slab models can be attributed to the small size of cluster models and the long-range non-directional nature of dispersion interactions. For this reason, the comparison between the cluster and slab results is performed below only with PBE.

The PBE adsorption binding energies are consistent with those from discrete cluster calculations under the provision that all H-bonds that form on the surfaces are adequately accounted for in cluster calculations. For imidazole, the binding energies for the $\text{Cu}(\text{OH})_2(001)$ slab and the $\text{Cu}(\text{OH})_2$ cluster are very similar, -0.37 eV and -0.39 eV, respectively, whereas for $(\text{CH}_3)_2\text{POOH}$ the results obtained with the $\text{Cu}(\text{OH})_2(001)$ slab and the $\text{Cu}(\text{OH})_2$ cluster are consistent only if all H-bonds are considered, i.e., the binding energy of -0.70 eV obtained on the surface is close to the sum of both H-bonds obtained from the cluster calculations, $-0.40 + (-0.37) = -0.77$ eV. Although the adsorption and cluster binding energies are compatible, the H-bond lengths are shorter on the $\text{Cu}(\text{OH})_2(001)$ surface.

The binding energy of imidazole on $\text{AlOOH}(010)$ is -0.43 eV, thus being similar to the value of -0.41 eV for the $\text{Al}(\text{OH})_3$ cluster. The slightly stronger interaction with the surface can be attributed in part to the stronger $\text{CH}\cdots\text{O}$ hydrogen bond because in the adsorption and cluster structures, this bond is formed with a different C atom of imidazole, i.e., the surface structure involves the stronger $\text{C2H}\cdots\text{O}$ bond, whereas the cluster structure involves the weaker $\text{C4H}\cdots\text{O}$ bond (for the corresponding bond strengths, see Fig. S2 in the Supplementary material).

For adsorption of $(\text{CH}_3)_2\text{POOH}$ on $\text{AlOOH}(010)$, two possible geometries were analyzed (Fig. 8). In the less stable structure, the $\text{P}=\text{O}$ group acts as an acceptor of two H-bonds with the surface OH groups and the resulting binding energy of -0.43 eV is less exothermic than the sum of the two corresponding H-bonds from the cluster calculations, which is $2 \times (-0.34) = -0.68$ eV. The reason for the inferior binding energy on the surface can be the rotation of one surface OH group during molecular adsorption, which costs about 0.2 eV (as estimated with the aid of a constrained relaxation calculation). Another reason can be due to the competitiveness effect [15] because two H-bonds are formed with the same functional group, which can reduce their strength. In the more stable structure ($E_b = -0.71$ eV), the $(\text{CH}_3)_2\text{POOH}$ molecule forms one H-bond with the $\text{P}=\text{O}$ group and another with the $\text{P}-\text{OH}$ group. This implies that $(\text{CH}_3)_2\text{POOH}$ acts as a donor and acceptor. For this structure, the results from the compatible discrete cluster calculation gives inferior binding energy of -0.60 eV. The difference arises from two additional longer $\text{OH}\cdots\text{O}$ hydrogen bonds present in the adsorption structure (indicated with gray color in Fig. 8) that further stabilize the structure and cannot be captured by simple cluster calculations. From auxiliary cluster calculations (Fig. S8), we estimate that these two longer H-bonds contribute $-0.2 + (-0.15) = -0.35$ eV. We also need to consider the cost for the rotation of one surface OH group, which costs about 0.2 eV. Summing all these contributions together gives $-0.60 - 0.35 + 0.2 = -0.75$ eV, which is a value very similar to the adsorption binding energy of -0.71 eV obtained on the $\text{AlOOH}(010)$ slab.

The comparison between the surface and cluster calculations therefore reveals that although small-cluster calculations can give reasonable estimates of adsorption energy provided that all formed H-bonds are adequately accounted for (which is not always trivial), there are, nevertheless, structural intricacies—such as additional “secondary” H-bonds that may form on the surface—that cannot be captured with small clusters.

Instead of accounting for all H-bonds present in the adsorption structure, let us now directly compare the most stable complexes obtained by the cluster and surface models. For $(\text{CH}_3)_2\text{POOH} + \text{Cu}(\text{OH})_2$, the strongest identified binding energy for the discrete cluster is -0.63 eV, whereas the adsorption binding energy is -0.70 eV. As for $\text{Al}(\text{OH})_3$, the strongest binding energies are -0.73 eV and -0.71 eV for the cluster and surface models, respectively. Since no structure information is included in this analysis, the similarity between the two types of binding energies is somewhat surprising, particularly for aluminum hydroxide. Although such a good agreement is likely serendipitous because only two metal hydroxides were considered, it shows that the strongest binding energy from cluster calculations can represent a reasonable estimate of the binding energy for molecules adsorbed via H-bonds.

For all adsorption structures, the electron charge density differences were calculated and are shown in Fig. 9 for imidazole and in Fig. 10 for $(\text{CH}_3)_2\text{POOH}$. Fig. 9 reveals that imidazole forms one strong $\text{OH}\cdots\text{N}$ hydrogen bond on the $\text{Cu}(\text{OH})_2(001)$ surface, whereas on the $\text{AlOOH}(010)$ surface, it also forms an additional $\text{C2H}\cdots\text{O}$ hydrogen bond. It is evident that the electron charge redistribution of the $\text{OH}\cdots\text{N}$ bond is higher on $\text{Cu}(\text{OH})_2(001)$ than on $\text{AlOOH}(010)$ hence the more exothermic binding energy on $\text{AlOOH}(010)$ is due to the additional $\text{C2H}\cdots\text{O}$ bond that is clearly visible in the charge density difference plot.

As for $(\text{CH}_3)_2\text{POOH}$, two H-bonds are formed between the molecule

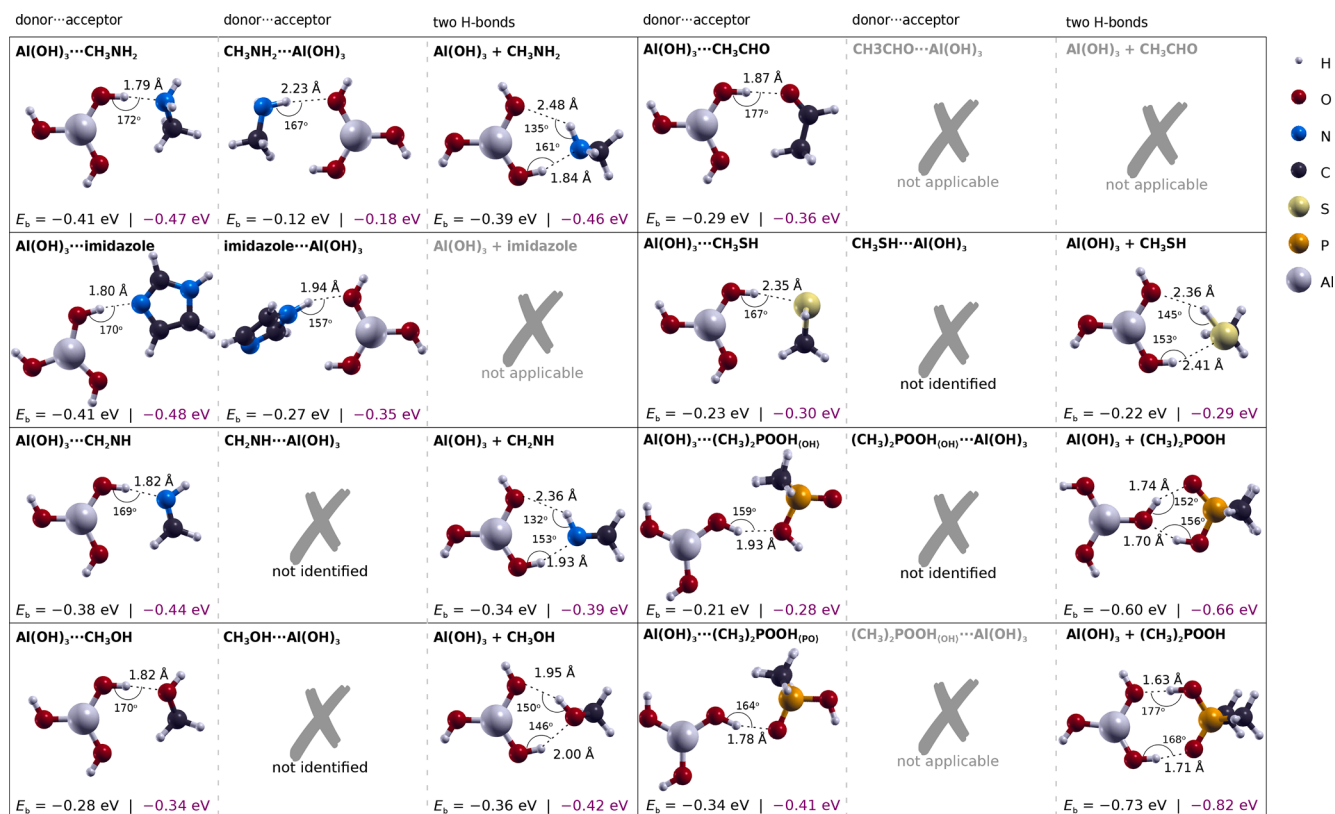


Fig. 6. Similar to Fig. 2, but for the H-bonded complexes with a discrete Al(OH)_3 cluster. Complexes for each molecule are divided into three columns: in the first column, the organic molecule acts as the H-bond acceptor and in the second as the H-bond donor. In the third column, the complexes with two hydrogen bonds are shown.

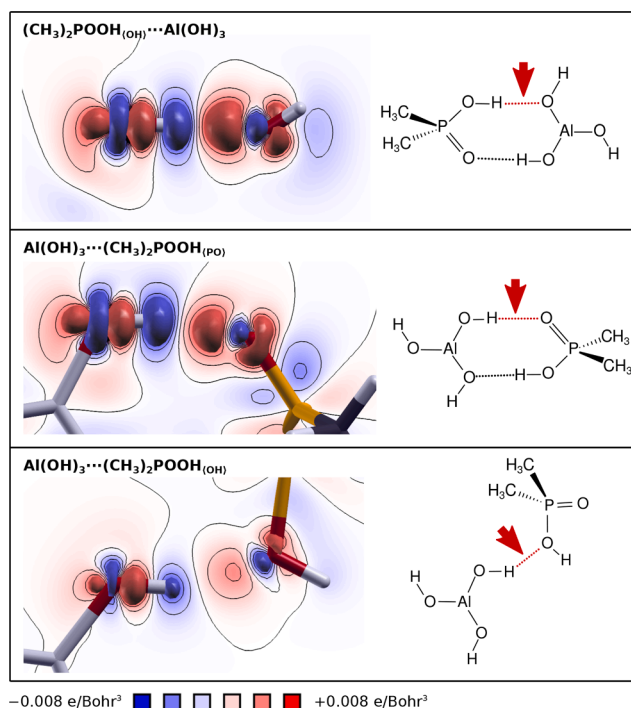


Fig. 7. The electron charge density difference, $\Delta\rho(r)$, for the three possible H-bonds that can form between $(\text{CH}_3)_2\text{POOH}$ and a discrete Al(OH)_3 cluster. For each case, the H-bond visualized in the $\Delta\rho(r)$ plot (left) is indicated by the red arrow on the schematic skeleton structure (right). Isosurfaces and contours are compatible with those shown in Figs. 3 and 5 (isosurfaces: $\pm 0.005 \text{ e/Bohr}^3$; contours: from -0.008 to 0.008 e/Bohr^3 with a linear increment of 0.002 e/Bohr^3).

and the $\text{Cu(OH)}_2(001)$ surface, which are visible in the charge density difference plots of Fig. 10; the two H-bonds are not on the same plane, hence they are shown separately. The H-bond where the P–OH group acts as a donor and the surface as the acceptor shows a noticeably higher electron charge density redistribution, hence it is stronger than the other H-bond, where the P=O group acts as an acceptor. This is also consistent with the H-bond lengths (Fig. 8).

In contrast, on $\text{AlOOH}(010)$, which has a more rigid structure, all H-bonds are formed in the same plane. The structure where the molecular P=O group acts as an acceptor of the two H-bonds with the surface OH groups is less stable than the structure where $(\text{CH}_3)_2\text{POOH}$ acts as both acceptor and donor. The electron charge density difference plots indeed reveal that the electron charge redistribution of the former structure is much lower than that of the latter structure. Further inspection of the inferior structure shows that the electron charge density redistribution is higher for the left H-bond; hence the two H-bonds are of different strength despite being of the same $\text{AlOH}\cdots\text{O}=\text{P}$ type. The difference in electron charge density redistribution for the two H-bonds is even more apparent for the superior adsorption structure. The $\text{POH}\cdots\text{O}(\text{H})\text{Al}$ hydrogen bond has a much higher electron charge density redistribution than the $\text{AlOH}\cdots\text{P}=\text{O}$ hydrogen bond. This is consistent with the fact that the $\text{POH}\cdots\text{O}(\text{H})\text{Al}$ hydrogen-bond is considerably shorter (Fig. 8). The two longer additional $\text{AlOH}\cdots\text{O}$ hydrogen bonds between the surface OH groups and the molecule, mentioned above, are also seen in Fig. 10 and it is evident that they are much weaker than the two shorter H-bonds.

3.6. H-bonding in the aqueous phase

The above analysis of H-bonding pertains to the vacuum phase, which is the simplest to study. However, the principal target of the current paper are H-bonding interactions between molecules and hy-

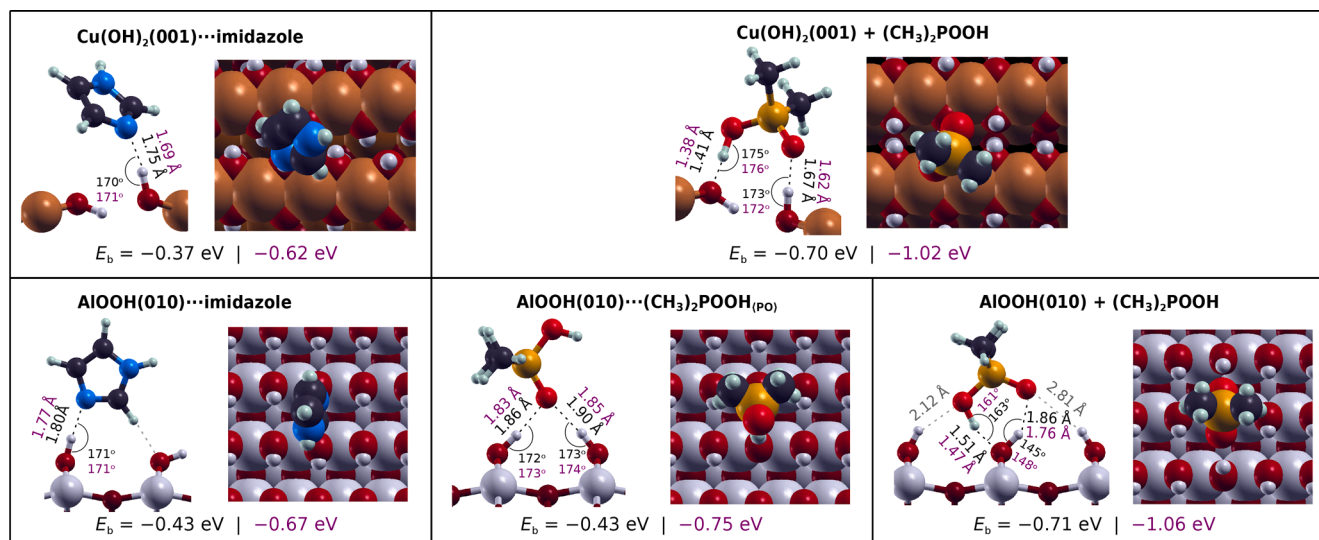


Fig. 8. The PBE optimized structures of imidazole (left) and $(\text{CH}_3)_2\text{POOH}$ (right) adsorbed via hydrogen bonding onto $\text{Cu(OH)}_2(001)$ (top row) and AlOOH(010) (bottom row); each adsorption structure is presented with side- and top-view snapshots. The corresponding binding energies, H-bond lengths, and H-bond angles are reported with the PBE values written in black and the PBE-D3 values written in purple.

droxylated surfaces, the latter being relevant in the aqueous phase. For this reason, we analyze below H-bonding interactions in the aqueous phase, which is treated implicitly by the continuum solvation model. To this end, the interactions of imidazole and $(\text{CH}_3)_2\text{POOH}$ molecules with Cu and Al substrates are considered. The corresponding aqueous phase results are compared to *in vacuo* results in Fig. 11. In general, the calculated binding energies are less exothermic in the aqueous phase. The E_b differences between aqueous and vacuum phases are usually smaller for complexes with one H-bond than for complexes with two H-bonds. The reason is obvious because, in the aqueous phase, the two constituents need to partly desolvate before interacting with each other. As for the H-bonding complexes with the Cu(OH)_2 and Al(OH)_3 clusters in the aqueous phase, the majority of complexes with a single H-bond show angles closer to 180° and shorter H-bond lengths than the vacuum phase analogs; note that stronger H-bonds tend to shorten more (for the trend, see Fig. 12a). There are only two exceptions where H-bonds elongate and in both Cu(OH)_2 acts as the donor, i.e., $\text{Cu(OH)}_2 \cdots (\text{CH}_3)_2\text{POOH}_{(\text{OH})}$ and $\text{Cu(OH)}_2 \cdots (\text{CH}_3)_2\text{POOH}_{(\text{PO})}$. Complexes with two H-bonds formed with the same OH group show elongation of the longer H-bond and shortening of the shorter H-bond, whereas for the complex between Al(OH)_3 and $(\text{CH}_3)_2\text{POOH}$, which involves different OH groups, both H-bonds shorten.

As for the H-bonding complexes with the $\text{Cu(OH)}_2(001)$ and AlOOH(010) surfaces in the aqueous phase, the H-bond lengths are either similar or slightly shorter than in the vacuum phase analogs. The most considerable discrepancy between aqueous and vacuum phases occurs for $(\text{CH}_3)_2\text{POOH}$ on $\text{Cu(OH)}_2(001)$ because in the aqueous phase $(\text{CH}_3)_2\text{POOH}$ spontaneously deprotonates (without a barrier), i.e., a proton shifts from the molecular OH group to a surface OH group, thus forming H_2O on the surface. Such barrierless deprotonation of $(\text{CH}_3)_2\text{POOH}$ was also observed on hydroxylated Cu(111) and $\text{Cu}_2\text{O(111)}$ [33]. In contrast, in the vacuum phase, such deprotonation does not occur (even if one starts from a “deprotonated” structure, the proton shifts back to the molecule during structural relaxation, as indicated by the inset in Fig. 11).

Similarly as reported above for the *in vacuo* results, the comparison between cluster and slab results of Fig. 11 reveals that in the aqueous phase, the binding energies obtained from discrete cluster calculations are consistent with the adsorption binding energies from slab calculations provided that all H-bonds that form on the surfaces are adequately accounted for in cluster calculations.

3.7. Relation between H-bond length and strength

The premise that stronger bonds are shorter is well established. This premise is also often utilized for H-bonds. A well known empirical relation between H-bond enthalpy (ΔH) and H-bond length (r) was put forward by Rozenberg et al. [65], which reads:⁴ $\Delta H = -1.558r^{-3.05}$, where ΔH is expressed in eV and r in Å units (r is the H...Y distance). This relation was derived from experimental data of cold isotopically diluted carbohydrate crystals. While the relation of Rozenberg et al. is based on H-bond enthalpies, our data are based on H-bond energies. However, the difference between the two is small at room temperature and is currently neglected.⁵

Fig. 12b shows the correlation between the PBE calculated binding energies and H-bond distances for the single H-bond molecular complexes solvated in implicit aqueous solvent (i.e., complexes from Fig. 11), whereas Fig. 12c shows the same correlation for single H-bond molecular complexes in vacuum (i.e., complexes from Figs. 2, 4, and 6). As for the complexes in implicit aqueous solvent (Fig. 12b), the data points display the trend compatible with the Rozenberg relation, although upshifted by about 0.05 to 0.1 eV (i.e., current H-bond energies are less exothermic), whereas the *in vacuo* results of Fig. 12c scatter around the Rozenberg curve. The larger scatter of datapoints in Fig. 12c compared to Fig. 12b can be attributed to a higher chemical diversity of considered complexes in vacuum (in addition to a single conventional H-bond, some complexes also contain a non-conventional CH...O hydrogen bond). Despite this scatter, the trend that stronger H-bonds tend to be shorter is apparent.

4. Conclusion

In summary, hydrogen bonding between two metal hydroxides, Al(OH)_3 and Cu(OH)_2 , and small organic molecules with functional groups containing N, O, S, or P heteroatoms was characterized using DFT calculations. To help contextualize the results, a water molecule was taken as a reference for evaluating H-bond characteristics. The presented

⁴ The original relation of Rozenberg et al. [65] is $\Delta H = -0.134r^{-3.05}$, where ΔH is expressed in kJ/mol and r in nm units.

⁵ For gas-phase complexes at room temperature, the difference between the two is $pV = RT = 26$ meV in magnitude, but for condensed phases, the difference is even smaller.

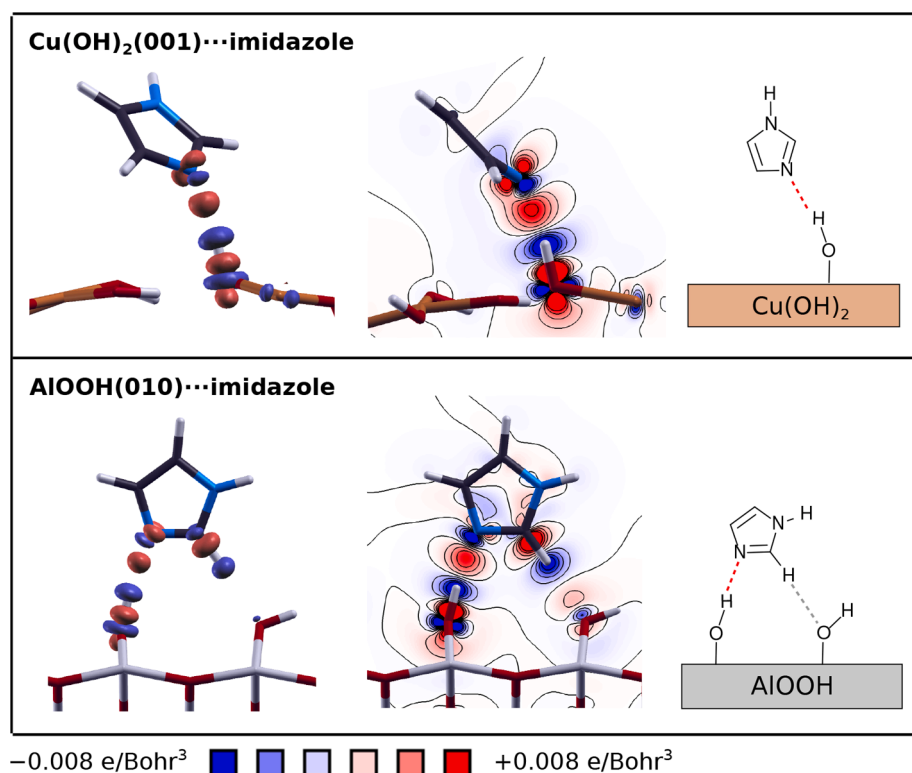


Fig. 9. The electron charge density difference for adsorption structures of imidazole. Isosurface and contour plots are shown separately. The plotted values are compatible with those shown in the other $\Delta\rho(\mathbf{r})$ figures (isosurfaces: $\pm 0.005 \text{ e}/\text{Bohr}^3$; contours: from -0.008 to $0.008 \text{ e}/\text{Bohr}^3$ with a linear increment of $0.002 \text{ e}/\text{Bohr}^3$).

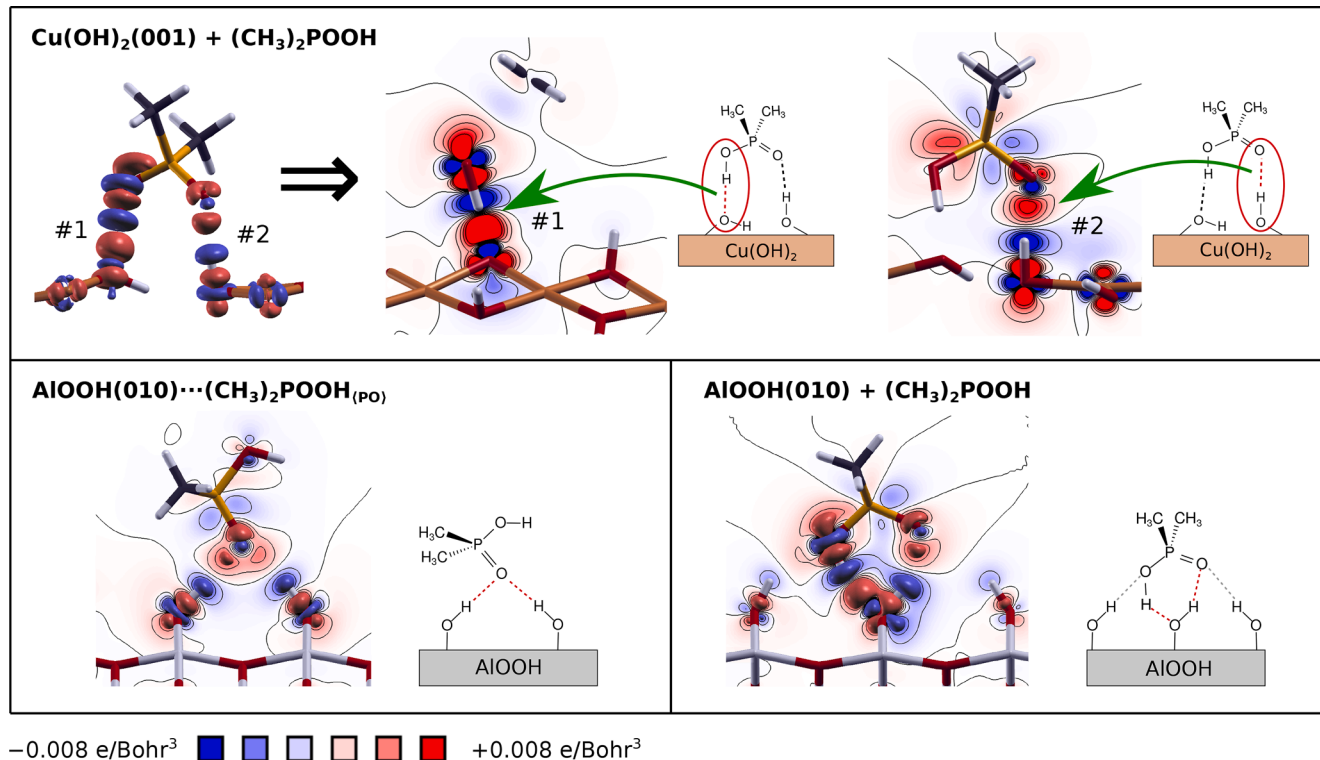


Fig. 10. The electron charge density difference for adsorption structures of $(\text{CH}_3)_2\text{POOH}$. H-bonds with $\text{Cu}(\text{OH})_2(001)$ lie in different planes, and the corresponding contour plots are therefore shown separately. Isosurfaces and contours are compatible with those shown in the other $\Delta\rho(\mathbf{r})$ figures (isosurfaces: $\pm 0.005 \text{ e}/\text{Bohr}^3$; contours: from -0.008 to $0.008 \text{ e}/\text{Bohr}^3$ with a linear increment of $0.002 \text{ e}/\text{Bohr}^3$).

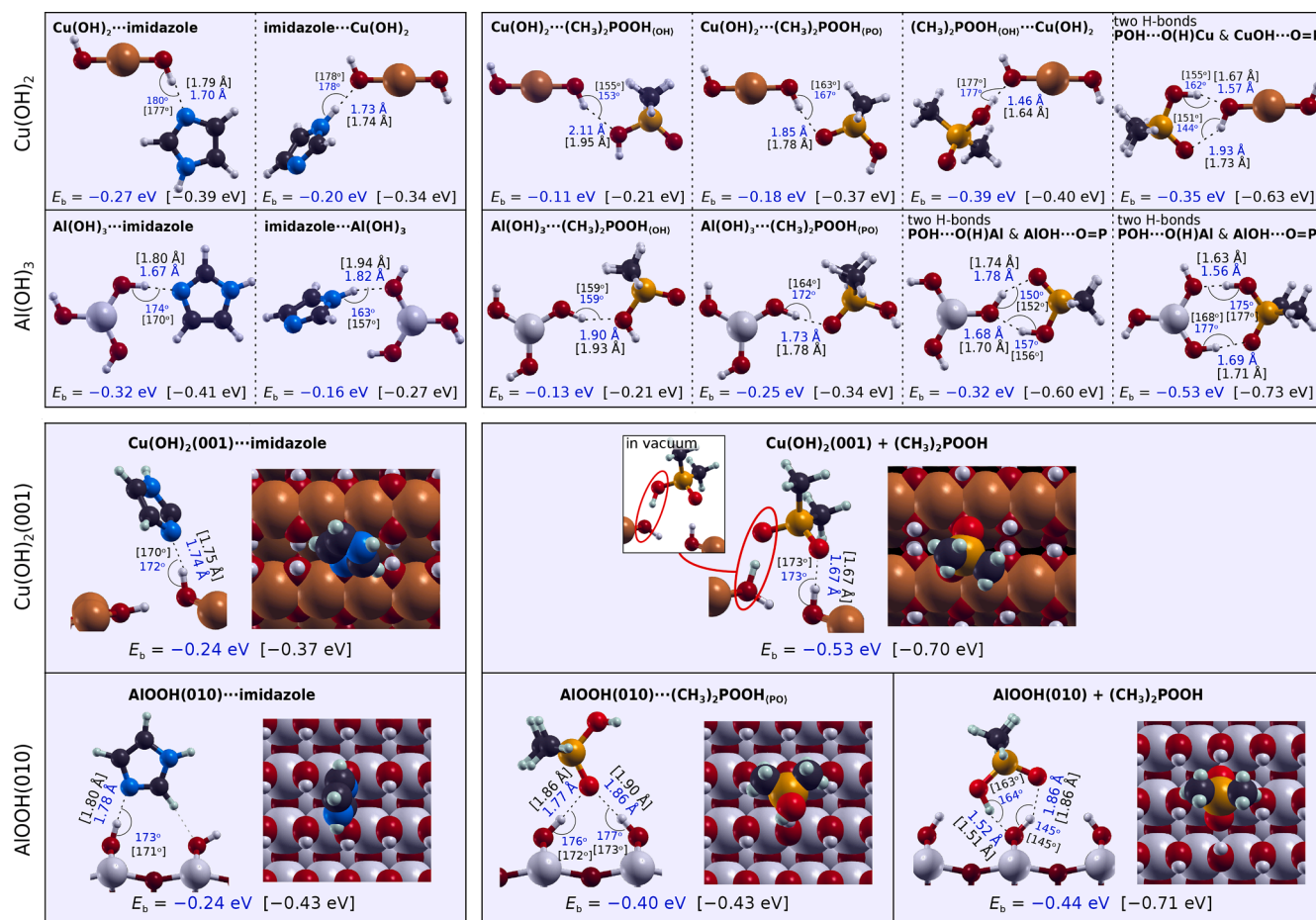


Fig. 11. The PBE optimized geometries, binding energies, H-bond lengths, and H-bond angles of imidazole (left) and $(\text{CH}_3)_2\text{POOH}$ (right) with Cu(OH)_2 and Al(OH)_3 clusters (top) and $\text{Cu(OH)}_2(001)$ and $\text{AlOOH}(010)$ surfaces (bottom) in implicit aqueous solvent. For comparison, the *in vacuo* results are written in the square brackets in black, whereas the aqueous phase values are written in blue. Note that $(\text{CH}_3)_2\text{POOH}$ deprotonates without a barrier on $\text{Cu(OH)}_2(001)$ with a proton shifting from the molecular OH group to a surface OH group, thus forming H_2O on the surface (in a vacuum, this deprotonation does not occur as indicated by the inset).

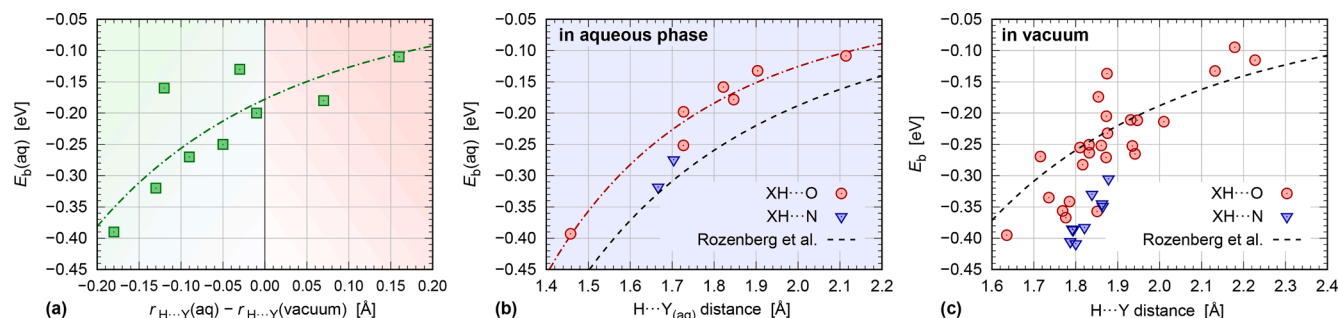


Fig. 12. (a) Aqueous phase PBE binding energies versus shortening of H-bonds in the aqueous phase compared to vacuum for molecular single H-bond complexes of Fig. 11. Note that stronger H-bonds tend to shorten more. (b,c) PBE H-bond energies versus H-bond lengths for aqueous and vacuum phases. In (b) molecular single H-bond complexes of Fig. 11 and in (c) single H-bond complexes of Figs. 2, 4, and 6 are considered. In (b,c), the empirical relation of Rozenberg et al. [65], $-1.558r^{-3.05}$ (see text) is shown by the black dashed curve, whereas the green dash-dotted curve in (a) and red curve in (b) are fitted to the $a r^{-b}$ relation.

calculations of the H-bonded complexes with discrete Al(OH)_3 and Cu(OH)_2 clusters showed that Cu(OH)_2 is usually a better H-bond donor and acceptor than a water molecule. The Al(OH)_3 cluster tends to form multiple hydrogen bonds with organic molecules, including weak $\text{CH} \cdots \text{O}$ bonds.

From the analysis of H-bond donor and acceptor propensities of functional groups containing N, O, S, and P heteroatoms, we can deduce that molecules with an N atom are very good H-bond acceptors, followed

by molecules containing an O atom, and then an S atom. The POOH group is also a very strong H-bond acceptor. In contrast, H-bond donor propensities depend more on the acidity of the hydrogen atom rather than the type of a heteroatom. When organic molecules act as H-bond acceptors, N-containing molecules display the following trend of H-bond strength with respect to hybridization of the N heteroatom: $\text{sp}^3 > \text{aromatic} > \text{sp}^2$. The dependence on the hybridization is similar but less pronounced for the O heteroatom, because in the considered cases, O

simultaneously acts as an H-bond donor and acceptor. Among the considered organic molecules, imidazole and $(\text{CH}_3)_2\text{POOH}$ form the strongest H-bonds. Imidazole has an aromatic character, and its pyridine-type N heteroatom is a very good H-bond acceptor, whereas its pyrrolic NH group is a good H-bond donor. Additionally, $(\text{CH}_3)_2\text{POOH}$ has a strong H-bond acceptor group ($\text{P}=\text{O}$) and a strong H-bond donor group (OH).

The H-bond propensity of the boehmite- $\text{AlOOH}(010)$ and $\text{Cu}(\text{OH})_2(001)$ surfaces are similar to their respective formula-unit $\text{Al}(\text{OH})_3$ and $\text{Cu}(\text{OH})_2$ clusters, although the molecule-cluster and molecule-surface binding energies can differ either due to the formation of additional H-bonds on surfaces or other structural intricacies. For example, the strongest identified binding energy between $(\text{CH}_3)_2\text{POOH}$ and the $\text{Cu}(\text{OH})_2$ cluster is -0.63 eV, whereas the respective value on the $\text{Cu}(\text{OH})_2(001)$ surface is -0.70 eV. Although in both cases $(\text{CH}_3)_2\text{POOH}$ acts as the H-bond donor and acceptor, the difference emerges because the bonding with the cluster involves one cluster OH group, and the bonding with the surface involves two surface OH groups. In contrast, for a few other cases, the binding energies obtained for clusters and surfaces are more similar. This implies that small-cluster calculations can give reasonable estimates of adsorption energy provided that all formed molecule-surface H-bonds are properly accounted for, which is not always trivial.

The effect of aqueous solvent was analyzed using the continuum solvation model. Considered H-bonds are usually shorter and their angles are closer to 180° in the aqueous solvent than in vacuum. Furthermore, the aqueous solvent may also promote deprotonation of adsorbed molecules, as observed for $(\text{CH}_3)_2\text{POOH}$ on $\text{Cu}(\text{OH})_2(001)$.

Declaration of Competing Interest

The authors declare that they have no known competing financial interests or personal relationships that could have appeared to influence the work reported in this paper.

Acknowledgments

This work has been financially supported by the Slovenian Research Agency (Grant No. P2-0393).

Appendix A. Supplementary material

Supplementary data associated with this article can be found, in the online version, at <https://doi.org/10.1016/j.chemphys.2022.111539>.

References

- [1] G.N. Lewis, *Valence and the Structure of Atoms and Molecules*, Chemical Catalog Com, New York, 1923.
- [2] L. Pauling, *The Nature of the Chemical Bond and the Structure of Molecules and Crystals*, Cornell University Press, Ithaca, New York, 1960.
- [3] H. Uneyama, K. Morokuma, The origin of hydrogen bonding. An energy decomposition study, *J. Am. Chem. Soc.* 99 (5) (1977) 1316–1332, <https://doi.org/10.1021/ja00447a007>.
- [4] G. Gilli, P. Gilli, Towards a unified hydrogen-bond theory, *J. Mol. Struct.* 552 (1–3) (2000) 1–15, [https://doi.org/10.1016/S0022-2860\(00\)00454-3](https://doi.org/10.1016/S0022-2860(00)00454-3).
- [5] G.R. Desiraju, T. Steiner, *The weak hydrogen bond: in structural chemistry and biology*, Vol. 9, International Union of Crystal, 2001.
- [6] S. Scheiner, S.J. Grabowski, T. Kar, Influence of hybridization and substitution on the properties of the $\text{CH}\cdots\text{O}$ hydrogen bond, *J. Phys. Chem. A* 105 (46) (2001) 10607–10612, <https://doi.org/10.1021/jp0131267>.
- [7] M. Domagala, S.J. Grabowski, $\text{CH}\cdots\text{N}$ and $\text{CH}\cdots\text{S}$ hydrogen bonds influence of hybridization on their strength, *J. Phys. Chem. A* 109 (25) (2005) 5683–5688, <https://doi.org/10.1021/jp0511496>.
- [8] A. Ebrahimi, M. Habibi-Khorassani, M. Doosti, F-H \cdots N hydrogen bonds: Influence of substituent and hybridization of nitrogen on H-bond properties and two-bond ^{19}F - ^{15}N spin-spin coupling constants ($^{2h}\text{J}_{\text{F-N}}$), *Chem. Phys. Lett.* 491 (1–3) (2010) 11–16, <https://doi.org/10.1016/j.cplett.2010.03.051>.
- [9] P. Gilli, L. Pretto, V. Bertolasi, G. Gilli, Predicting hydrogen-bond strengths from acid-base molecular properties. the pK_a slide rule: Toward the solution of a long-lasting problem, *Acc. Chem. Res.* 42 (1) (2008) 33–44, <https://doi.org/10.1021/ar800001k>.
- [10] J. Laskowski, Q. Liu, C. O'Connor, Current understanding of the mechanism of polysaccharide adsorption at the mineral/aqueous solution interface, *Int. J. Miner. Process.* 84 (1–4) (2007) 59–68, <https://doi.org/10.1016/j.minpro.2007.03.006>.
- [11] K. Norén, P. Persson, Adsorption of monocarboxylates at the water/goethite interface: The importance of hydrogen bonding, *Geochim. Cosmochim. Acta* 71 (23) (2007) 5717–5730, <https://doi.org/10.1016/j.gca.2007.04.037>.
- [12] S. Irrera, D. Costa, K. Ogle, P. Marcus, Molecular modelling by DFT of 1,2-diaminoethane adsorbed on the Zn-terminated and O-terminated, anhydrous and hydroxylated $\text{ZnO}(0001)$ surface, *Superlattices Microstruct.* 46 (1) (2009) 19–24, <https://doi.org/10.1016/j.spmi.2008.11.021>.
- [13] M. Poberžnik, F. Chiter, I. Milošev, P. Marcus, D. Costa, A. Kokalj, DFT study of n-alkyl carboxylic acids on oxidized aluminum surfaces: from standalone molecules to self-assembled-monolayers, *Appl. Surf. Sci.* 525 (2020) 146156, <https://doi.org/10.1016/j.apsusc.2020.146156>.
- [14] M. Poberžnik, D. Costa, A. Hemeryck, A. Kokalj, Insight into the bonding of silanols to oxidized aluminum surfaces, *J. Phys. Chem. C* 122 (17) (2018) 9417–9431, <https://doi.org/10.1021/acs.jpcc.7b12552>.
- [15] H. Lutz, Structure and strength of hydrogen bonds in inorganic solids, *J. Mol. Struct.* 646 (1–3) (2003) 227–236, [https://doi.org/10.1016/S0022-2860\(02\)00716-0](https://doi.org/10.1016/S0022-2860(02)00716-0).
- [16] H.D. Lutz, Hydroxide ions in condensed materials — correlation of spectroscopic and structural data, in: *Coordination Chemistry*, Springer, Berlin, Heidelberg, 1995, pp. 85–103, <https://doi.org/10.1007/BFb0036826>.
- [17] H.D. Lutz, Bonding and structure of water molecules in solid hydrates. Correlation of spectroscopic and structural data, in: *Solid Materials*, Springer, Berlin, Heidelberg, 1988, pp. 97–125, https://doi.org/10.1007/3-540-18790-1_3.
- [18] H. Lutz, K. Beckenkamp, H. Möller, Weak hydrogen bonds in solid hydroxides and hydrates, *J. Mol. Struct.* 322 (1994) 263–266, [https://doi.org/10.1016/0022-2860\(94\)87043-8](https://doi.org/10.1016/0022-2860(94)87043-8).
- [19] J. Smets, W. McCarthy, G. Maes, L. Adamowicz, Correlations between ab initio and experimental data for isolated 1:1 hydrogen-bonded complexes of pyridine and imidazole derivatives with water, *J. Mol. Struct.* 476 (1–3) (1999) 27–43, [https://doi.org/10.1016/S0022-2860\(98\)00536-5](https://doi.org/10.1016/S0022-2860(98)00536-5).
- [20] P. Raybaud, M. Digne, R. Iftimie, W. Wellens, P. Euzen, H. Toulhoat, Morphology and surface properties of boehmite (γ - AlOOH): a density functional theory study, *J. Catal.* 201 (2) (2001) 236–246, <https://doi.org/10.1006/jcat.2001.3246>.
- [21] M. Digne, P. Sautet, P. Raybaud, P. Euzen, H. Toulhoat, Hydroxyl groups on γ -alumina surfaces: A DFT study, *J. Catal.* 211 (1) (2002) 1–5, <https://doi.org/10.1006/jcat.2002.3741>.
- [22] B.F. Ngouana-Wakou, P. Cornette, M. Corral Valero, D. Costa, P. Raybaud, An atomistic description of the γ -alumina/water interface revealed by ab initio molecular dynamics, *J. Phys. Chem. C* 121 (19) (2017) 10351–10363, <https://doi.org/10.1021/acs.jpcc.7b00101>.
- [23] A. Motta, M.-P. Gaigeot, D. Costa, Ab Initio Molecular Dynamics Study of the AlOOH Boehmite/Water Interface: Role of Steps in Interfacial Groththus Proton Transfers, *J. Phys. Chem. C* 116 (23) (2012) 12514–12524, <https://doi.org/10.1021/jp3000812>.
- [24] M. Sassi, Z. Wang, E.D. Walter, X. Zhang, H. Zhang, X.S. Li, A. Tuladhar, M. Bowden, H.-F. Wang, S.B. Clark, K.M. Rosso, Surface Hydration and Hydroxyl Configurations of Gibbsite and Boehmite Nanoplates, *J. Phys. Chem. C* 124 (9) (2020) 5275–5285, <https://doi.org/10.1021/acs.jpcc.0c00659>.
- [25] A.G. Medvedev, A.A. Mikhaylov, I.Yu. Chernyshov, M.V. Vener, O. Lev, P. V. Prikhodchenko, Effect of aluminum vacancies on the H_2O_2 or H_2O interaction with a gamma- AlOOH surface. A solid-state DFT study, *Int. J. Quantum Chem.* 119 (13) (2019) e25920, <https://doi.org/10.1002/qua.25920>.
- [26] A. Motta, M.-P. Gaigeot, D. Costa, AIMD Evidence of Inner Sphere Adsorption of Glycine on a Stepped (101) Boehmite AlOOH Surface, *J. Phys. Chem. C* 116 (44) (2012) 23418–23427, <https://doi.org/10.1021/jp307565p>.
- [27] T. Ribeiro, A. Motta, P. Marcus, M.-P. Gaigeot, X. Lopez, D. Costa, Formation of the OOH radical at steps of the boehmite surface and its inhibition by gallic acid: A theoretical study including DFT-based dynamics, *J. Inorg. Biochem.* 128 (2013) 164–173, <https://doi.org/10.1016/j.jinorgbio.2013.07.024>.
- [28] T. Bauer, T. Schmaltz, T. Lenz, M. Halik, B. Meyer, T. Clark, Phosphonate- and carboxylate-based self-assembled monolayers for organic devices: A theoretical study of surface binding on aluminum oxide with experimental support, *ACS Appl. Mater. Inter.* 5 (13) (2013) 6073–6080, <https://doi.org/10.1021/am4008374>.
- [29] M. Poberžnik, A. Kokalj, Implausibility of bidentate bonding of the silanol headgroup to oxidized aluminum surfaces, *Appl. Surf. Sci.* 492 (2019) 909–918, <https://doi.org/10.1016/j.apsusc.2019.04.032>.
- [30] A. Kokalj, Corrosion inhibitors: physisorbed or chemisorbed? *Corros. Sci.* 196 (2022) 109939, <https://doi.org/10.1016/j.corsci.2021.109939>.
- [31] X. Yu, X. Zhang, S. Wang, G. Feng, A computational study on water adsorption on $\text{Cu}_2\text{O}(111)$ surfaces: The effects of coverage and oxygen defect, *Appl. Surf. Sci.* 343 (2015) 33–40, <https://doi.org/10.1016/j.apsusc.2015.03.065>.
- [32] X. Yu, X. Zhang, H. Wang, G. Feng, High coverage water adsorption on the $\text{CuO}(111)$ surface, *Appl. Surf. Sci.* 425 (2017) 803–810, <https://doi.org/10.1016/j.apsusc.2017.07.086>.
- [33] D.K. Kozlica, A. Kokalj, I. Milošev, Synergistic effect of 2-mercaptobenzimidazole and octylphosphonic acid as corrosion inhibitors for copper and aluminium – An electrochemical, XPS, FTIR and DFT study, *Corros. Sci.* 182 (2021) 109082, <https://doi.org/10.1016/j.corsci.2020.109082>.
- [34] J.P. Perdew, K. Burke, M. Ernzerhof, Generalized gradient approximation made simple, *Phys. Rev. Lett.* 77 (18) (1996) 3865–3868, <https://doi.org/10.1103/PhysRevLett.77.3865>.

- [35] D. Vanderbilt, Soft self-consistent pseudopotentials in a generalized eigenvalue formalism, *Phys. Rev. B* 41 (1990) 7892–7895, <https://doi.org/10.1103/PhysRevB.41.7892>.
- [36] Ultrasoft pseudopotentials for H, C, N, O, Al, P, and Cu atoms were taken from the Quantum ESPRESSO Pseudopotential Download Page at <http://www.quantum-espresso.org/pseudopotentials> (files: H.pbe-rrkjus.UPF, C.pbe-rrkjus.UPF, N.pbe-rrkjus.UPF, O.pbe-rrkjus.UPF, Al.pbe-rrkjus_psl.0.1.UPF, P.pbe-rrkjus_psl.0.1.UPF, and Cu.pbe-rrkjus.UPF). (2021).
- [37] P. Giannozzi, S. Baroni, N. Bonini, M. Calandra, R. Car, C. Cavazzoni, D. Ceresoli, G.L. Chiarotti, M. Cococcioni, I. Dabo, A. Dal Corso, S. de Gironcoli, S. Fabris, G. Fratesi, R. Gebauer, U. Gerstmann, C. Gougousis, A. Kokalj, M. Lazzeri, L. Martin-Samos, N. Marzari, F. Mauri, R. Mazzarello, S. Paolini, A. Pasquarello, L. Paulatto, C. Sbraccia, S. Scandolo, G. Sclauzero, A.P. Seitsonen, A. Smogunov, P. Umari, R. M. Wentzcovitch, Quantum ESPRESSO: a modular and open-source software project for quantum simulations of materials, *J. Phys: Condens. Matter* 21 (39) (2009) 395502, code available from <http://www.quantum-espresso.org/>, <https://doi.org/10.1088/0953-8984/21/39/395502>.
- [38] P. Giannozzi, O. Andreussi, T. Brumme, O. Bunau, M.B. Nardelli, M. Calandra, R. Car, C. Cavazzoni, D. Ceresoli, M. Cococcioni, N. Colonna, I. Carnimeo, A. Dal Corso, S. de Gironcoli, P. Delugas, R. DiStasio, A. Ferretti, A. Floris, G. Fratesi, G. Fugallo, R. Gebauer, U. Gerstmann, F. Giustino, T. Gorni, J. Jia, M. Kawamura, H.-Y. Ko, A. Kokalj, E. Küçükbenli, M. Lazzeri, M. Marsili, N. Marzari, F. Mauri, N. L. Nguyen, H.-V. Nguyen, A.O. de-la-Roza, L. Paulatto, S. Poncè, D. Rocca, R. Sabatini, B. Santra, M. Schlipf, A.P. Seitsonen, A. Smogunov, I. Timrov, T. Thonhauser, P. Umari, N. Vast, X. Wu, S. Baroni, Advanced capabilities for materials modelling with Quantum ESPRESSO, *J. Phys: Condens. Matter* 29 (2017) 465901, <https://doi.org/10.1088/1361-648X/aa8f79>.
- [39] S. Grimme, J. Antony, S. Ehrlich, H. Krieg, A consistent and accurate ab initio parametrization of density functional dispersion correction (DFT-D) for the 94 elements H-Pu, *J. Chem. Phys.* 132 (15) (2010) 154104, <https://doi.org/10.1063/1.3382344>.
- [40] G. Makov, M.C. Payne, Periodic boundary conditions in ab initio calculations, *Phys. Rev. B* 51 (7) (1995) 4014–4022, <https://doi.org/10.1103/PhysRevB.51.4014>.
- [41] G.D. Purvis III, R.J. Bartlett, A full coupled-cluster singles and doubles model: The inclusion of disconnected triples, *J. Chem. Phys.* 76 (4) (1982) 1910–1918, <https://doi.org/10.1063/1.443164>.
- [42] F. Weigend, R. Ahlrichs, Balanced basis sets of split valence, triple zeta valence and quadruple zeta valence quality for H to Rn: Design and assessment of accuracy, *Phys. Chem. Chem. Phys.* 7 (18) (2005) 3297–3305, <https://doi.org/10.1039/B508541A>.
- [43] M.J. Frisch, G.W. Trucks, H.B. Schlegel, G.E. Scuseria, M.A. Robb, J.R. Cheeseman, G. Scalmani, V. Barone, G.A. Petersson, H. Nakatsuji, X. Li, M. Caricato, A.V. Marenich, J. Bloino, B.G. Janesko, R. Gomperts, B. Mennucci, H.P. Hratchian, J.V. Ortiz, A.F. Izmaylov, J.L. Sonnenberg, D. Williams-Young, F. Ding, F. Lipparini, F. Egidi, J. Goings, B. Peng, A. Petrone, T. Henderson, D. Ranasinghe, V.G. Zakrzewski, J. Gao, N. Rega, G. Zheng, W. Liang, M. Hada, M. Ehara, K. Toyota, R. Fukuda, J. Hasegawa, M. Ishida, T. Nakajima, Y. Honda, O. Kitao, H. Nakai, T. Vreven, K. Throssell, J.A. Montgomery, Jr., J.E. Peralta, F. Ogliaro, M.J. Bearpark, J.J. Heyd, E.N. Brothers, K.N. Kudin, V.N. Staroverov, T.A. Keith, R. Kobayashi, J. Normand, K. Raghavachari, A.P. Rendell, J.C. Burant, S.S. Iyengar, J. Tomasi, M. Cossi, J.M. Millam, M. Klene, C. Adamo, R. Cammi, J.W. Ochterski, R.L. Martin, K. Morokuma, O. Farkas, J.B. Foresman, D.J. Fox, Gaussian 16 Revision B.01, gaussian Inc., Wallingford CT (2016).
- [44] S.F. Boys, F.d. Bernardi, The calculation of small molecular interactions by the differences of separate total energies. Some procedures with reduced errors, *Mol. Phys.* 19 (4) (1970) 553–566, <https://doi.org/10.1080/00268977000101561>.
- [45] S. Simon, M. Duran, J. Dannenberg, How does basis set superposition error change the potential surfaces for hydrogen-bonded dimers? *J. Chem. Phys.* 105 (24) (1996) 11024–11031, <https://doi.org/10.1063/1.472902>.
- [46] H.R. Oswald, A. Reller, H.W. Schmalke, E. Dubler, Structure of copper(II) hydroxide, Cu(OH)₂, *Acta Crystallogr. Sect. C: Cryst. Struct. Commun.* 46 (12) (1990) 2279–2284, <https://doi.org/10.1107/S0108270190006230>.
- [47] N. Marzari, D. Vanderbilt, A. De Vita, M.C. Payne, Thermal contraction and disordering of the Al(110) surface, *Phys. Rev. Lett.* 82 (16) (1999) 3296–3299, <https://doi.org/10.1103/PhysRevLett.82.3296>.
- [48] O. Andreussi, I. Dabo, N. Marzari, Revised self-consistent continuum solvation in electronic-structure calculations, *J. Chem. Phys.* 136 (6) (2012) 064102, <https://doi.org/10.1063/1.3676407>.
- [49] G. Fiscaro, L. Genovese, O. Andreussi, S. Mandal, N.N. Nair, N. Marzari, S. Goedecker, Soft-sphere continuum solvation in electronic-structure calculations, *J. Chem. Theory Comput.* 13 (8) (2017) 3829–3845, <https://doi.org/10.1021/acs.jctc.7b00375>.
- [50] A. Kokalj, Computer graphics and graphical user interfaces as tools in simulations of matter at the atomic scale, *Comp. Mater. Sci.* 28 (2) (2003) 155–168, [https://doi.org/10.1016/S0927-0256\(03\)00104-6](https://doi.org/10.1016/S0927-0256(03)00104-6), proceedings of the Symposium on Software Development for Process and Materials Design.
- [51] Inkscape Project, Inkscape, version 0.92.4 (2019). URL: <https://inkscape.org>.
- [52] A.D. Boese, J.M. Martin, W. Klopper, Basis set limit coupled cluster study of H-bonded systems and assessment of more approximate methods, *J. Phys. Chem. A* 111 (43) (2007) 11122–11133, <https://doi.org/10.1021/jp072431a>.
- [53] D.D. Nelson Jr., G.T. Fraser, W. Klemperer, Does ammonia hydrogen bond? *Science* 238 (1987) 1670–1674, <https://doi.org/10.1126/science.238.4834.1670>.
- [54] S. Raub, C.M. Marian, Quantum chemical investigation of hydrogen-bond strengths and partition into donor and acceptor contributions, *J. Comput. Chem.* 28 (9) (2007) 1503–1515, <https://doi.org/10.1002/jcc.20673>.
- [55] E.Y. Tupikina, M. Bodensteiner, P.M. Tolstoy, G.S. Denisov, I.G. Shenderovich, P=O moiety as an ambidextrous hydrogen bond acceptor, *J. Phys. Chem. C* 122 (3) (2018) 1711–1720, <https://doi.org/10.1021/acs.jpcc.7b11299>.
- [56] P.R. Rablen, J.W. Lockman, W.L. Jorgensen, Ab initio study of hydrogen-bonded complexes of small organic molecules with water, *J. Phys. Chem. A* 102 (21) (1998) 3782–3797, <https://doi.org/10.1021/jp980708o>.
- [57] J.S. Arey, P.C. Aeberhard, I.-C. Lin, U. Rothlisberger, Hydrogen bonding described using dispersion-corrected density functional theory, *J. Phys. Chem. B* 113 (14) (2009) 4726–4732, <https://doi.org/10.1021/jp810323m>.
- [58] A. Mandal, M. Prakash, R.M. Kumar, R. Parthasarathi, V. Subramanian, Ab initio and DFT studies on methanol-water clusters, *J. Phys. Chem. A* 114 (6) (2010) 2250–2258, <https://doi.org/10.1021/jp909397z>.
- [59] J. Schwöbel, R.-U. Ebert, R. Kühne, G. Schüürmann, Prediction of the intrinsic hydrogen bond acceptor strength of chemical substances from molecular structure, *J. Phys. Chem. A* 113 (37) (2009) 10104–10112, <https://doi.org/10.1021/jp904812b>.
- [60] J. Schwöbel, R.-U. Ebert, R. Kühne, G. Schüürmann, Prediction of the intrinsic hydrogen bond acceptor strength of organic compounds by local molecular parameters, *J. Chem. Inf. Model.* 49 (4) (2009) 956–962, <https://doi.org/10.1021/ci900040z>.
- [61] Y. Gu, T. Kar, S. Scheiner, Fundamental properties of the CH...O interaction: Is it a true hydrogen bond? *J. Am. Chem. Soc.* 121 (40) (1999) 9411–9422, <https://doi.org/10.1021/ja991795g>.
- [62] D. Gustinić, A. Kokalj, A DFT study of adsorption of imidazole, triazole, and tetrazole on oxidized copper surfaces: Cu₂O(111) and Cu₂O(111)-w/o-Cu^{CUS}, *Phys. Chem. Chem. Phys.* 17 (2015) 28602–28615, <https://doi.org/10.1039/C5CP03647J>.
- [63] D. Gustinić, A. Kokalj, DFT study of azole corrosion inhibitors on Cu₂O model of oxidized copper surfaces: II. Lateral interactions and thermodynamic stability, *Metals* 8 (5) (2018) 311, <https://doi.org/10.3390/met8050311>.
- [64] N. Kovačević, I. Milošević, A. Kokalj, How relevant is the adsorption bonding of imidazoles and triazoles for their corrosion inhibition of copper? *Corros. Sci.* 124 (2017) 25–34, <https://doi.org/10.1016/j.corsci.2017.04.021>.
- [65] M. Rozenberg, A. Loewenschuss, Y. Marcus, An empirical correlation between stretching vibration redshift and hydrogen bond length, *Phys. Chem. Chem. Phys.* 2 (12) (2000) 2699–2702, <https://doi.org/10.1039/B002216K>.